PALLADIUM NANOFILM GROWTH AND SURFACE MODIFICATION FOR ENHANCED HYDROGEN DESORPTION KINETICS BY ELECTROCHEMICAL ATOMIC LAYER DEPOSITION (E-ALD) AND DEVELOPMENT OF ELECTROLESS ATOMIC LAYER DEPOSITION (EL-ALD)

by

KAUSHIK JAGANNATHAN

(Under the Direction of John L. Stickney)

ABSTRACT

This dissertation describes electrodeposition and electroless deposition of Pd. Pd thin films were grown by E-ALD on polycrystalline Au substrates. A scheme to modify the surface of the Pd with Pt was developed. The films were grown by surface limited redox replacement (SLRR). As the name suggests, surface limited reactions are used to grow conformal, thin films with precise coverage and controlled thickness. An atomic layer of Cu (sacrificial metal) was deposited at an underpotential and then replaced by Pd ions (noble metal) to form an atomic layer of Pd. This process was repeated to grow Pd thin films of the desired coverage. Following this, Cu was deposited at an underpotential on the Pd surface and then replaced by Pt ions to modify the Pd surface with Pt metal. The coverage was varied by tuning the UPD potential. Hydrogen sorption was studied by cyclic voltammetry (CV). Based on the CV, a scheme to charge and discharge the films with hydrogen using coulometry was developed. Enhancements in the rate of hydrogen desorption compared to bare Pd was observed even with low Pt coverage. In addition, the films maintained the ability to store hydrogen. Based on the results, an indirect

mechanism for hydrogen sorption is proposed. Oxygen reduction in the films was also studied and an enhancement in the kinetics is reported.

Electroless deposition involves the ability to deposit metal without applying any current. The technique is versatile and can be used on a variety of substrates. A two-step method for electroless atomic layer deposition (EL-ALD) of Pd was developed. Initially, Sn ions are adsorbed and then replaced by Pd ions in an SLRR reaction. CV was used to optimize the sequence and quantify the amount of Sn present. Deposition on Au, ITO, FTO and glass was achieved. EL-ALD Pd deposition was three times less than with E-ALD. AFM indicates a nucleation and growth model. Cu electrodeposited on Pd sensitized ITO was investigated and indicates a weak interaction between Pd and ITO under high currents. Pd deposition was found to be constant from cycle to cycle for EL-ALD just as in E-ALD.

INDEX WORDS: Underpotential, Surface limited reactions, E-ALD, EL-ALD, UPD, SLRR electrodeposition, electroless deposition, nanofilm, Pd, Pt, hydrogen storage, kinetics, mechanism, oxygen reduction, sensitization, activation, cyclic voltammetry, coulometry, SEM, AFM

PALLADIUM NANOFILM GROWTH AND SURFACE MODIFICATION FOR ENHANCED HYDROGEN DESORPTION KINETICS BY ELECTROCHEMICAL ATOMIC LAYER DEPOSITION (E-ALD) AND DEVELOPMENT OF ELECTROLESS ATOMIC LAYER DEPOSITION (EL-ALD)

by

KAUSHIK JAGANNATHAN

B.Sc., S.I.E.S College of Arts, Science and Commerce (University of Mumbai), India, 2008

M.Sc., Ramnarain Ruia College (University of Mumbai), India, 2010

A Dissertation Submitted to the Graduate Faculty of The University of Georgia in Partial Fulfillment of the Requirements for the Degree

DOCTOR OF PHILOSOPHY

ATHENS, GEORGIA

2015

PALLADIUM NANOFILM GROWTH AND SURFACE MODIFICATION FOR ENHANCED HYDROGEN DESORPTION KINETICS BY ELECTROCHEMICAL ATOMIC LAYER DEPOSITION (E-ALD) AND DEVELOPMENT OF ELECTROLESS ATOMIC LAYER DEPOSITION (EL-ALD)

by

KAUSHIK JAGANNATHAN

Major Professor:	John L. Stickney
Committee:	Tina Salguero
	Gary Douberly

Electronic Version Approved:

Suzanne Barbour
Dean of the Graduate School
The University of Georgia
December 2015

DEDICATION

This dissertation is dedicated to my incredible parents, Mr. Jagannathan Raghavachari and Mrs. Malathy Jagannathan, my loving grandparents, my caring wife Purva and my amazing sister Gayathri. Whatever I am today is because of you. Thank you for everything you have done.

ACKNOWLEDGEMENTS

My parents have always put our education first and made a lot of sacrifices for me to reach this stage in my life. Their hard work and simplicity has been an inspiration to push myself and do my best. My beautiful, supportive wife has always believed in my abilities even when I have lost faith. She kept me on track and focused on the end goal and has been there every time I needed her support. My grandparents, Mrs. Rukmini Raghvachari (Paati), Mr. M.S. Kannan (Thatha) and Mrs. Lakshmi Kannan (Babi) have shown me what it means to be selfless. I have never met my grandfather Mr. Raghavachari, but everything I have heard about him has been inspiring. My achievements today will make them incredibly happy wherever they are. Having a sister who has always looked up to me has motivated me to never give up. I am also incredibly lucky to have the most caring and supportive parents- in-laws and sister- in -law. The love they have for each other and everyone around them is amazing.

I would like to extend my gratitude to members of Prof. John L. Stickney's group, especially Dr. Leah Sheridan for training me during my early days. I would also like to thank my committee members Dr. Tina Salguero and Dr. Gary Douberly, and my collaborator Dr. David Robinson for their guidance and support. Finally, I would like to thank Prof. John L. Stickney without whom none of this would have been possible. He has been an amazing advisor and more important, a very caring and supportive mentor.

TABLE OF CONTENTS

Page

LIST OF FIGURES

page

CHAPTER 1

INTRODUCTION AND LITERATURE REVIEW

With the current growth in areas such as microelectronics and fuel cells, thin films have become an important area of research. Conventionally, there exist several different techniques to grow these films. Broadly, these can be classified into two categories. The first category being physical processes such as molecular beam epitaxy (MBE) [1-4] and electron beam deposition and the second based on chemical techniques such as such as sol gel coatings, metalloorganic chemical vapor deposition (MOCVD) [5-8], chemical vapor deposition (CVD) [9-11], physical vapor deposition (PVD) [12], vapor phase epitaxy (VPE) [13], atomic layer deposition (ALD), electrodeposition and electroless deposition. The advantage of electrodeposition and electroless deposition techniques over vacuum techniques are that they are comparatively easier and economical, and usually do not need expensive equipment like ultra high vacuum (UHV) systems. In particular, electrochemical atomic layer deposition (E-ALD) offers an alternative to traditional gas phase atomic layer deposition. The first reports of E-ALD were by the author's group. At the time the technique was referred to as electrochemical atomic layer epitaxy (EC-ALE) [14-33]. A major advantage of this technique over gas phase ALD is the ability to grow films at room temperature and pressure. E-ALD can be used to conformally grow films, one atomic layer at a time. An atomic layer is defined as a one atom thick layer that is a monolayer (ML) or less. A monolayer is a unit of coverage defined as one deposit atom per substrate atom. Similar to gas phase ALD, E-ALD also

uses surface limited reactions (SLRs) to control the amount of metal deposited. SLRs in solution involve the underpotential deposition (UPD) of a metal. UPD is a thermodynamic phenomenon which involves depositing a metal at a potential prior to (under) that needed to deposit on itself. Hence, the potential for deposition must be lower than the formal potential (E^0) for bulk deposition. UPD is possible because the depositing metal is more stable on another metal (i.e. the substrate). The farther away the UPD potential is from the formal potential, the lower the amount of metal deposited.

Typically, in E-ALD, an atomic layer of a sacrificial metal is deposited at an underpotential. Depending on the system studied, the sacrificial metal is replaced by a more noble metal at open circuit. The noble metal ions donate electrons to the sacrificial metal. This results in a surface limited redox replacement (SLRR) process where the sacrificial metal is oxidized and the noble metal is reduced. SLRR was initially introduced as monolayer restricted galvanic displacement (MRGD) by Adzic and coworkers [34] and later on referred to as SLRR [35]. Dimitrov et al. then achieved epitaxial growth by SLRR in a single three compartment electrochemical set up by immersing in different solutions [36].

Active research is being currently carried out for moving towards a "hydrogen economy". Hydrogen is being considered as a viable alternative to fossil fuels because its combustion is clean. In order for widespread use of hydrogen as a fuel source to become a reality, it is essential to address challenges in the storage of hydrogen.

Hydrogen can be stored from the gas phase or electrochemically [37]. Hydrogen sorption is a fundamentally important reaction and is important for applications involving the kinetics of the reaction as well as for understanding the durability of the system.

Materials based storage is one approach for hydrogen storage. The different categories of materials for storage are sorbents, chemical hydrogen storage, metals and alloys.

Sorbents are porous materials and have a very high surface area [38-42] and can be metal organic frameworks (MOFs) or carbon based sorbents. Carbon sorbents have a diverse array of structures such as fullerenes, aerogels, molecular sieves [43] or carbon nanotubes [44]. MOFs consist of metal building blocks linked by organic molecules [45]. Zn and Cu are typically used for the metal centers but there are other transition metals in use as well [46, 47]. The hydrogen uptake is related to a number of factors such as dipole moments, co-ordination sites for the hydrogen to occupy and surface area of the material [48]. Typically, the mechanism proposed is a spill over mechanism where the H_2 dissociates at the surface and then moves into the underlying substrate. There have been many successful constructs to reversibly store hydrogen in MOFs. However, they are typically susceptible to moisture [47] and can decompose in the presence of acids and bases [49]. In addition both carbon and MOF based sorbents have very weak Van der Waals interactions between the hydrogen and the substrate. This in turn requires cryogenic operating temperatures [50].

Complex hydrides used in hydrogen storage consist of metal atoms covalently bound to anionic hydrogen containing counter ions such as $[BH_4]^-$, $[NH_2]^-$ or $[AlH_4]^-$ [51]. However, they suffer from various drawbacks such as slow kinetics, lack of reversibility, and undesirable side reactions such as evolution of ammonia and diboranes and low capacity [52].

Hydrogen can also be stored in transition metals and some alkali metals forming a non stoichiometric compound (MH_x). Switendick showed that these are distinct from

solid solutions by studying their band structures [53]. A major advantage of metal hydrides is the ability to store hydrogen at room temperature and pressure [54]. These are the simplest class of materials capable of hydrogen storage. They are typically MH_x, with x = 1, or 2, or 3. In the case of transition metals, the hydrogen reversibly occupies interstitial sites in the fcc crystal without changing the crystal structure and hence, these compounds are also called interstitial hydrides. Palladium is one such metal which is capable of storing hydrogen reversibly in the bulk and on its surface, although it is an anomaly to the typical MH_x formula since x is less than 1 for Pd. Detailed discussions on hydrogen storage are presented in chapter 2.

This thesis describes Pd electrodeposition by electrochemical atomic layer deposition (chapter 2) as well as electroless atomic layer deposition (chapter 3). In electroless deposition, no external current is required and deposition can occur from aqueous solutions, non- aqueous solutions and melts [55]. Pd can be deposited by electroless deposition using a two -step sensitization and activation process. Deposition can also occur from electrochemical baths such as hydrazine [56-58] and hypophosphite [59, 60] baths. Ohno has described in detail the composition and the disadvantages of these baths in a review [61]. Another method of deposition involves sensitizing a substrate followed by an activation step [62]. The process involves the adsorption of Sn ions (sensitization) followed by replacement by Pd (activation). The activated substrate can then be used for further treatment with a variety of metals. Cu filling in vias was studied by Lau et al. where the Cu was deposited on Pd activated substrates [63]. Ang et al. decorated carbon nanotubes with copper and nickel by applying the sensitization-activation process in two steps as described above, and in a

single step by adsorption of Sn-Pd alloys from a single solution containing Sn and Pd ions [64]. Zhu et al. improved the performance of PtRu/C catalysts by pretreating the carbon particles by a sensitization-activation step [65]. The effect of UV radiation on the Pd activation process has been reported by Baylis et al. [66].

Chapter 2 describes hydrogen storage in Pt modified Pd films. The Pd was deposited on polycrystalline Au substrates using a previously optimized sequence [67, 68]. Bimetallic catalysts can show enhanced catalytic abilities [69], in some cases even more so than monometallic catalysts [70]. A procedure to modify the surface of the Pd with Pt is described. The Pd coverage was kept constant at 2.5 ML, while varying amounts of Pt was electrodeposited directly on the E-ALD Pd films. This was achieved by SLRR of Cu_{UPD}. The coverage of Pt was tuned by varying the potential applied for UPD of Cu. Cyclic voltammetry (CV) was used to investigate the potentials where adsorption and absorption occurred on the bare and Pt modified Pd thin films. Based on the CVs, a potential sequence was developed to electrochemically charge and discharge the films with hydrogen. The effect of surface modification with Pt on hydrogen absorption was investigated. In order to study the kinetics for hydrogen desorption, the hydrogen oxidation current-time traces were compared for bare and Pt modified Pd films. There was significant increases in the currents even with very low Pt coverages on the Pd surface. Curve fittings with a simple biexponential function were carried out in the decay region of the hydrogen oxidation current-time traces. This resulted in two time constants corresponding to two independent processes, hydrogen absorption and adsorption. Desorption rates of over a magnitude higher than for bare Pd films were obtained even with very low Pt coverages. Based on the ability to differentiate between bulk and

surface hydride, as well as trends seen in a time constant vs. coverage plot, possible mechanisms for hydrogen desorption are discussed.

Chapter 3 introduces a new technique, electroless atomic layer deposition (EL-ALD). One advantage of this technique is the ability to deposit controlled amounts of Pd without applying any external current, as mentioned earlier. This allows deposition to occur on a variety of conducting (metals), semi conducting (transparent conductive oxides) and insulating surfaces (glass). In the present work, deposition on Au, FTO, ITO and glass is compared by using electrochemistry and microscopy techniques wherever applicable. Deposits were grown in a two-step process. First, Sn^{2+} ions were introduced into the flow cell and were adsorbed for a fixed period of time. After a rinse step to remove any excess or weakly bound Sn^{2+} ions, Pd^{2+} ions were pumped into the flow cell. An SLRR process occurred where the Sn^{2+} is oxidized to Sn^{4+} by gaining 2 electrons from Pd^{2+}. This results in Pd^{2+} is reduced to Pd^{0}. The process is repeated multiple times to form Pd films on the substrate. Pd deposits were grown on FTO, ITO and Au in this fashion. To determine the coverage as a function of cycle number, the Pd was then stripped electrochemically. Early reports indicate a linear growth process very similar to E-ALD. In order to study the nucleation sites and understand, the growth model, deposition was carried out on glass slides in the E-ALD flow cell system. The deposits were then imaged by atomic force microscopy (AFM) and the height distribution was studied as a function of coverage.

Appendix A describes studies involving the oxygen reduction reaction (ORR). Pd films were deposited on polycrystalline Au and their surface was modified with varying amounts of Pt as described in chapter 2. Cyclic voltammetry was used to study the onset

of oxygen reduction in palladium. This was compared to the effect of the presence of Pt on the Pd surface. It was found that the presence of Pt on the surface reduced the overpotential for O_2 reduction into Pd. Possible mechanisms are discussed and interpreted based on the voltammetry.

References

1. Goldstein, L., et al., *Growth by molecular beam epitaxy and characterization of InAs/GaAs strained-layer superlattices.* Applied Physics Letters, 1985. **47**(10): p. 1099-1101.
2. Chen, Y., et al., *Plasma assisted molecular beam epitaxy of ZnO on c-plane sapphire: growth and characterization.* Journal of Applied Physics, 1998. **84**(7): p. 3912-3918.
3. Chen, Y., et al., *Growth of ZnO single crystal thin films on c-plane (0 0 0 1) sapphire by plasma enhanced molecular beam epitaxy.* Journal of crystal growth, 1997. **181**(1): p. 165-169.
4. Murakami, M., et al., *Anatase TiO2 thin films grown on lattice-matched LaAlO3 substrate by laser molecular-beam epitaxy.* Applied Physics Letters, 2001. **78**: p. 2664.
5. Choi, B.J., et al., *Cyclic PECVD of Ge2Sb2Te5 films using metallorganic sources.* Journal of the Electrochemical Society, 2007. **154**(4): p. H318-H324.
6. Yang, J.L., et al., *Photocatalysis using ZnO thin films and nanoneedles grown by metal–organic chemical vapor deposition.* Advanced materials, 2004. **16**(18): p. 1661-1664.

7. Kim, R.-Y., H.-G. Kim, and S.-G. Yoon, *Structural properties of Ge2Sb2Te5 thin films by metal organic chemical vapor deposition for phase change memory applications.* Applied physics letters, 2006. **89**(10): p. 2107.

8. Kapolnek, D., et al., *Structural evolution in epitaxial metalorganic chemical vapor deposition grown GaN films on sapphire.* Applied Physics Letters, 1995. **67**(11): p. 1541-1543.

9. Suzuki, K., et al., *Growth of diamond thin films by dc plasma chemical vapor deposition.* Applied physics letters, 1987. **50**(12): p. 728-729.

10. Reina, A., et al., *Large area, few-layer graphene films on arbitrary substrates by chemical vapor deposition.* Nano letters, 2008. **9**(1): p. 30-35.

11. Barreca, D., et al., *Composition and microstructure of cobalt oxide thin films obtained from a novel cobalt (II) precursor by chemical vapor deposition.* Chemistry of Materials, 2001. **13**(2): p. 588-593.

12. Narayan, J., et al., *Epitaxial growth of TiN films on (100) silicon substrates by laser physical vapor deposition.* Applied physics letters, 1992. **61**(11): p. 1290-1292.

13. Stringfellow, G., *Fundamental aspects of organometallic vapor phase epitaxy.* Materials Science and Engineering: B, 2001. **87**(2): p. 97-116.

14. Vaidyanathan, R., J.L. Stickney, and U. Happek, *Quantum confinement in PbSe thin films electrodeposited by electrochemical atomic layer epitaxy (EC-ALE).* Electrochimica Acta, 2004. **49**(8): p. 1321-1326.

15. Kim, Y.-G., et al., *Platinum nanofilm formation by EC-ALE via redox replacement of UPD copper: studies using in-situ scanning tunneling microscopy.* The Journal of Physical Chemistry B, 2006. **110**(36): p. 17998-18006.

16. Varazo, K., et al., *Formation of the first monolayers of CdTe on Au (111) by electrochemical atomic layer epitaxy (EC-ALE): studied by LEED, Auger, XPS, and in-situ STM.* Journal of Electroanalytical Chemistry, 2002. **522**(1): p. 104-114.

17. Mathe, M.K., et al., *Deposition of CdSe by EC-ALE.* Journal of crystal growth, 2004. **271**(1): p. 55-64.

18. Venkatasamy, V., et al., *Optimization of CdTe nanofilm formation by electrochemical atomic layer epitaxy (EC-ALE).* Journal of applied electrochemistry, 2006. **36**(11): p. 1223-1229.

19. Muthuvel, M. and J.L. Stickney, *CdTe electrodeposition on InP (100) via electrochemical atomic layer epitaxy (EC-ALE): studies using UHV-EC.* Langmuir, 2006. **22**(12): p. 5504-5508.

20. Venkatasamy, V., et al., *Deposition of HgTe by electrochemical atomic layer epitaxy (EC-ALE).* Journal of Electroanalytical Chemistry, 2006. **589**(2): p. 195-202.

21. Venkatasamy, V., et al., *Optimization studies of HgSe thin film deposition by electrochemical atomic layer epitaxy (EC-ALE).* Electrochimica acta, 2006. **51**(21): p. 4347-4351.

22. Wade, T.L., et al., *Electrochemical formation of a III–V compound semiconductor superlattice: InAs/InSb.* Journal of Electroanalytical Chemistry, 2001. **500**(1): p. 322-332.

23. Vaidyanathan, R., et al., *Formation of In_2Se_3 thin films and nanostructures using electrochemical atomic layer epitaxy.* Journal of Electroanalytical Chemistry, 2003. **559**: p. 55-61.

24. Flowers, B.H., et al., *Atomic layer epitaxy of CdTe using an automated electrochemical thin-layer flow deposition reactor.* Journal of Electroanalytical Chemistry, 2002. **524**: p. 273-285.

25. Vaidyanathan, R., et al. *Electrodeposition of Cu_2Se thin films by Electrochemical Atomic Layer Epitaxy (EC-ALE)*. in *MRS Proceedings*. 2002. Cambridge Univ Press.

26. Gregory, B.W., D.W. Suggs, and J.L. Stickney, *Conditions for the deposition of CdTe by electrochemical atomic layer epitaxy.* Journal of the Electrochemical Society, 1991. **138**(5): p. 1279-1284.

27. Zhu, W., et al., *Optimization of the formation of bismuth telluride thin film by using ECALE.* Journal of Electroanalytical Chemistry, 2005. **585**(1): p. 83-88.

28. Mathe, M.K., et al., *Formation of HgSe thin films using electrochemical atomic layer epitaxy.* Journal of The Electrochemical Society, 2005. **152**(11): p. C751-C755.

29. Gichuhi, A., B.E. Boone, and C. Shannon, *Electrosynthesized CdS/HgS heterojunctions.* Langmuir, 1999. **15**(3): p. 763-766.

30. Foresti, M., et al., *Electrochemical atomic layer epitaxy deposition of CdS on Ag (111): An electrochemical and STM investigation.* The Journal of Physical Chemistry B, 1998. **102**(38): p. 7413-7420.

31. Colletti, L.P. and J.L. Stickney, *Optimization of the growth of CdTe thin films formed by electrochemical atomic layer epitaxy in an automated deposition system.* Journal of the Electrochemical Society, 1998. **145**(10): p. 3594-3602.

32. Lister, T.E., L.P. Colletti, and J.L. Stickney, *Electrochemical formation of CdSe monolayers on the low index planes of Au.* Israel journal of chemistry, 1997. **37**(2-3): p. 287-295.

33. Demir, U. and C. Shannon, *Electrochemistry of Cd at (√3×√3)R30°-S/Au(111): Kinetics of Structural Changes in CdS Monolayers.* Langmuir, 1996. **12**(25): p. 6091-6097.

34. Brankovic, S., J. Wang, and R. Adžić, *Metal monolayer deposition by replacement of metal adlayers on electrode surfaces.* Surface Science, 2001. **474**(1): p. L173-L179.

35. Mrozek, M.F., Y. Xie, and M.J. Weaver, *Surface-Enhanced Raman Scattering on Uniform Platinum-Group Overlayers: Preparation by Redox Replacement of Underpotential-Deposited Metals on Gold.* Analytical Chemistry, 2001. **73**(24): p. 5953-5960.

36. Viyannalage, L.T., R. Vasilic, and N. Dimitrov, *Epitaxial Growth of Cu on Au(111) and Ag(111) by Surface Limited Redox ReplacementAn Electrochemical and STM Study.* The Journal of Physical Chemistry C, 2007. **111**(10): p. 4036-4041.

37. Jerkiewicz, G. and A. Zolfaghari, *Comparison of hydrogen electroadsorption from the electrolyte with hydrogen adsorption from the gas phase.* Journal of The Electrochemical Society, 1996. **143**(4): p. 1240-1248.

38. Dinca, M., et al., *Hydrogen storage in a microporous metal-organic framework with exposed Mn^{2+} coordination sites.* Journal of the American Chemical Society, 2006. **128**(51): p. 16876-16883.

39. Frost, H., T. Düren, and R.Q. Snurr, *Effects of surface area, free volume, and heat of adsorption on hydrogen uptake in metal-organic frameworks.* The Journal of Physical Chemistry B, 2006. **110**(19): p. 9565-9570.

40. Germain, J., J.M.J. Frechet, and F. Svec, *Hypercrosslinked polyanilines with nanoporous structure and high surface area: potential adsorbents for hydrogen storage.* Journal of Materials Chemistry, 2007. **17**(47): p. 4989-4997.

41. Germain, J., et al., *High Surface Area Nanoporous Polymers for Reversible Hydrogen Storage.* Chemistry of Materials, 2006. **18**(18): p. 4430-4435.

42. Collins, D.J. and H.-C. Zhou, *Hydrogen storage in metal–organic frameworks.* Journal of materials chemistry, 2007. **17**(30): p. 3154-3160.

43. Hynek, S., W. Fuller, and J. Bentley, *Hydrogen storage by carbon sorption.* International Journal of Hydrogen Energy, 1997. **22**(6): p. 601-610.

44. Poirier, E., et al., *Hydrogen adsorption measurements and modeling on metal-organic frameworks and single-walled carbon nanotubes.* Langmuir, 2006. **22**(21): p. 8784-8789.

45. Rowsell, J.L. and O.M. Yaghi, *Strategies for hydrogen storage in metal–organic frameworks.* Angewandte Chemie International Edition, 2005. **44**(30): p. 4670-4679.

46. Suh, M.P., et al., *Hydrogen Storage in Metal–Organic Frameworks.* Chemical Reviews, 2012. **112**(2): p. 782-835.

47. Deng, H., et al., *Large-pore apertures in a series of metal-organic frameworks.* science, 2012. **336**(6084): p. 1018-1023.

48. Murray, L.J., M. Dinca, and J.R. Long, *Hydrogen storage in metal-organic frameworks.* Chemical Society Reviews, 2009. **38**(5): p. 1294-1314.

49. Kang, I.J., et al., *Chemical and thermal stability of isotypic metal–organic frameworks: effect of metal ions.* Chemistry-A European Journal, 2011. **17**(23): p. 6437-6442.

50. Yang, J., et al., *High capacity hydrogen storage materials: attributes for automotive applications and techniques for materials discovery.* Chemical Society Reviews, 2010. **39**(2): p. 656-675.

51. Ley, M.B., et al., *Complex hydrides for hydrogen storage – new perspectives.* Materials Today, 2014. **17**(3): p. 122-128.

52. Orimo, S.-i., et al., *Complex Hydrides for Hydrogen Storage.* Chemical Reviews, 2007. **107**(10): p. 4111-4132.

53. Switendick, A., *The change in electronic properties on hydrogen alloying and hydride formation*, in *Hydrogen in Metals I*. 1978, Springer. p. 101-129.

54. Züttel, A., *Materials for hydrogen storage.* Materials Today, 2003. **6**(9): p. 24-33.

55. Djokić, S.S. and P.L. Cavallotti, *Electroless deposition: theory and applications*, in *Electrodeposition*. 2010, Springer. p. 251-289.

56. Shu, J., et al., *Autocatalytic effects in electroless deposition of palladium.* Journal of The Electrochemical Society, 1993. **140**(11): p. 3175-3180.

57. Rhoda, R., *Electroless plating with precious metals.* Plating, 1963. **50**: p. 307.

58. Hsu, C. and R.E. Buxbaum, *Electroless and immersion plating of palladium on zirconium.* Journal of the Electrochemical Society, 1985. **132**(10): p. 2419-2420.

59. Pearlstein, F. and R. Weightman, *Electroless Palladium Deposition.* Plating, 1969. **56**(10): p. 1158-61.

60. Mizumoto, S., et al., *Electroless Plating of Pd--P Alloys From Ethylenediamine Complex Solutions.* Hyomen Gijutsu(J. Surf. Finish. Soc. Jpn.), 1989. **40**(3): p. 477-480.

61. Ohno, I., *Electroless deposition of palladium and platinum.* Modern Electroplating, Fifth Edition, 2010: p. 477-482.

62. Shipley, J.C.R., *Method of electroless deposition on a substrate and catalyst solution therefor*. U.S. Patent 3011920, 1961.

63. Lau, P., C. Wong, and L. Chan, *Improving electroless Cu via filling with optimized Pd activation.* Applied Surface Science, 2006. **253**(5): p. 2357-2361.

64. Ang, L.M., et al., *Decoration of activated carbon nanotubes with copper and nickel.* Carbon, 2000. **38**(3): p. 363-372.

65. Zhu, J., et al., *Improving the performance of PtRu/C catalysts for methanol oxidation by sensitization and activation treatment.* Journal of Power Sources, 2007. **166**(2): p. 331-336.

66. Baylis, B., C.C. Huang, and M. Schlesinger, *A Study of the Products of Ultraviolet Irradiation of Palladium-Containing Catalysts for Electroless Metal Deposition.* Journal of The Electrochemical Society, 1979. **126**(3): p. 394-397.

67. Sheridan, L.B., et al., *Electrochemical Atomic Layer Deposition (E-ALD) of Palladium Nanofilms by Surface Limited Redox Replacement (SLRR), with EDTA Complexation.* Electrocatalysis, 2012. **3**(2): p. 96-107.

68. Sheridan, L.B., et al., *Formation of Palladium Nanofilms Using Electrochemical Atomic Layer Deposition (E-ALD) with Chloride Complexation.* Langmuir, 2013. **29**(5): p. 1592-1600.

69. Croy, J.R., et al., *Bimetallic Pt-Metal catalysts for the decomposition of methanol: Effect of secondary metal on the oxidation state, activity, and selectivity of Pt.* Applied Catalysis A: General, 2008. **350**(2): p. 207-216.

70. Jordão, M.H., V. Simões, and D. Cardoso, *Zeolite supported Pt-Ni catalysts in n-hexane isomerization.* Applied Catalysis A: General, 2007. **319**: p. 1-6.

CHAPTER 2

HYDROGEN SORPTION AND ITS KINETICS ON BARE AND PLATINUM-MODIFIED PALLADIUM NANOFILMS GROWN BY ELECTROCHEMICAL ATOMIC LAYER DEPOSITION (E-ALD)

---

[1]Kaushik Jagannathan, David Benson, David B. Robinson, John L. Stickney, To be submitted to *Journal of Materials Chemistry A*

Abstract

Pd nanofilms were grown on polycrystalline Au substrates using the electrochemical version of atomic layer deposition (E-ALD). Multiple cycles of surface-limited redox replacement (SLRR) were used to grow deposits, where each SLRR cycle involved the underpotential deposition (UPD) of a Cu atomic layer, followed by its open circuit replacement via redox exchange with tetrachloropalladate, forming a Pd atomic layer. That process constitutes one E-ALD deposition cycle. The cycle was repeated in order to grow deposits of the desired thickness. In the present study, 5 cycles of Pd deposition were performed on polycrystalline Au on glass substrates, resulting in the formation of 2.5 monolayers of Pd. Those Pd films were then modified with varying coverages of Pt, also formed using SLRR. The amount of Pt was controlled by changing the potential for Cu UPD during the Pt SLRR, and by increasing the number of Pt deposition cycles performed. Hydrogen absorption was studied using coulometry and cyclic voltammetry in 0.1 M H_2SO_4 as a function of the Pt coverage. The presence of even a small fraction of a Pt monolayer increased the rate of hydrogen desorption. However, the presence of Pt on the Pd surface did not reduce its ability to store hydrogen. Desorption rates for hydrogen from Pt modified films were over an order of magnitude faster than those for Pd alone.

Introduction

Hydrogen is a valuable fuel for transportation purposes because its energy can be harvested efficiently and it does not generate air pollution in the vicinity of the vehicle. Challenges associated with the compact storage of hydrogen remain an obstacle to its widespread use [1]. Storage in the form of a solid hydride is one way to achieve a high volumetric energy density. While too expensive for automotive hydrogen storage, palladium (Pd) is an often studied material for this purpose due to its high reversibility to charge-discharge cycles, its resistance to oxidation and the low hydrogen gas overpressure required to maintain the hydride state [2]. Pd forms a surface hydride as well as a non-stoichiometric compound PdH_x in the bulk when hydrogen atoms occupy octahedral sites in the fcc crystal lattice [3]. Moreover, the formation of the hydride can occur at room temperature and atmospheric pressure. This ability of Pd to store hydrogen on its surface or in the bulk thus opens up avenues in sensing [4] and in the storage of hydrogen, as well as a component of fuel cell catalysts [5].

Electrochemical atomic layer deposition (E-ALD) is the electrochemical version of gas phase ALD. It can be performed at room temperature and used to grow deposits one atomic layer at a time. E-ALD has been used to grow semiconductors and superlattice films [6, 7]. Initially, E-ALD was developed by growing compound semiconductors [8-12]. With the introduction of surface limited redox replacement (SLRR) [13-15], E-ALD became applicable to the growth of metal nanofilms as well. SLRR involves the initial deposition of an atomic layer of a sacrificial metal using

underpotential deposition (UPD) [16], followed by exchange of the UPD layer for a more noble metal via redox replacement with its ionic precursor at open circuit, completing one E-ALD cycle. The cycle can then be repeated as necessary to produce conformal nanofilms of a desired thickness.

Pd electrodeposition has been studied extensively on Au substrates by various groups. For example, Kibler et al. [17] studied the deposition of Pd on Au from chloride containing solutions, while Brankovic et al. [18] were the first to study Pd deposition on Au(111) using SLRR: with Cu UPD as the sacrificial atomic layer. No preferential Pd deposition was observed on steps or defect sites.

One early report of hydrogen absorption in Pd was by Flanagan et al. [19] who studied the progress of hydrogen absorption in palladium wires and noticed that surface processes influenced the absorption of hydrogen. Baldauf and Kolb [20] grew ultrathin Pd layers on Au(111) and studied hydrogen sorption in those films. Quaino et al. [21] used theoretical models to study hydrogen oxidation on submonolayers of Pd on Au(111) and correlated changes in electronic properties and geometric arrangements.

Surface modification has been known to have an effect on the electroactivity of Pd. Czerwinski et al. [22] reported the influence of CO on the absorption and desorption of hydrogen. Baldauf and Kolb showed that the presence of crystal violet enhances the hydrogen absorption reaction [20]. Bartlett and Marwan report the same effect with crystal violet as well as Pt [23]. Sheridan et al. studied hydrogen sorption into Rh modified Pd films and reported a kinetic enhancement [24].

A scheme for the growth of Pd films on Au polycrystalline and single crystal substrates was developed by groups that included authors of this article, and used to study hydrogen sorption [25-27]. That work demonstrated the ability to achieve flat, uniform, conformal layers over the deposit area. In the present work, the controlled growth of Pd nanofilms on polycrystalline Au substrates, as well as surface modification with Pt using E-ALD, will be described. Those deposits have been used here to extend observations of Bartlett and Marwan [23]. The Pd films maintain the amount of hydrogen stored, even while covered with Pt, while demonstrating higher peak currents for hydrogen desorption. The kinetics of hydrogen desorption from a Pd crystal lattice were studied using coulometry, and the rate constants for hydrogen desorption have been calculated, as have those when the surface has been modified by fractions of a monolayer of Pt. Considering these results, and those from other recent work concerning the enhanced kinetics resulting from Pt surface modification, possible mechanisms are briefly discussed based on the ability to differentiate surface hydride adsorption and bulk hydride absorption in the Pd thin films.

Experimental

Vapor deposited Au on glass slides (100 nm Au on a 5 nm Ti adhesion layer) were used as substrates for all deposits (EMF Corporation). Solutions were prepared with 18 MΩ-cm ultrapure water (Milli-Q Advantage A10). The Pd solution was 0.1 mM ultrapure-grade $PdCl_2$ (Aldrich Chemicals) in 50 mM HCl, in which the

tetrachloropalladate ion $PdCl_4^{2-}$ is expected to form. The Pt solution was 0.01 mM ultrapure-grade H_2PtCl_6 (Aldrich Chemicals) in 50 mM $HClO_4$. The Cu solution was 1 mM $CuSO_4$ (J.T. Baker Chemical Co., 99.8%) and 0.1 M H_2SO_4. The deposits were grown and studied in an automated electrochemical flow deposition system (Electrochemical ALD L.C., Athens, GA), diagramed in Figure 2.1. The system consisted of five solution reservoirs, 5 valves and a variable speed peristaltic pump. The valves were housed in a Plexiglas box along with the solution reservoirs so they could be purged continuously with N_2, to minimize exposure to O_2. The electrochemical flow cell, downstream from the valves, was also made of Plexiglas and had a volume of around 0.15 mL. A three electrode cell configuration was used, with a gold wire auxiliary electrode embedded in the front cell plate, directly across from the substrate. The reference was an Ag/AgCl electrode (3M KCl) from Bioanalytical systems, against which potentials have been reported. E-ALD software "Sequencer-4" was used to control valves, pump and potentials. The Au on glass substrates had an exposed area of 0.71 cm^2, defined using a Polydonut masking tape (EPSI).

Results and Discussions

Formation of nanofilms by E-ALD: Prior to deposition, the Au substrate was cleaned by cycling in 0.1 M H_2SO_4 from -0.2 V to 1.4 V 3 times at 10 mV/s, followed by 2 cycles in 50mM HCl from -0.2 V to 0.7 V at 10 mV/s, to produce a more ordered surface [27]. Figure 2.2 is a schematic for the SLRR deposition of Pd, and surface

modification of the Pd nanofilms with Pt. The E-ALD cycle for Pd deposition was optimized and studied previously by this group [24-27]. E-ALD has also been used to grow Pt nanofilms on Au [15, 28]. The Pt E-ALD cycle, used in this study, was modified in order to deposit controlled fractions of a monolayer on the Pd nanofilms. Figure 2.2 represents the formation of a Pd thin film on a Au slide. Initially an atomic layer of Cu is deposited on Au. This is followed by a redox replacement of the Cu by Pd^{2+} ions at open circuit resulting in an atomic layer of Pd metal. The cycle is repeated to form a Pd thin film. This is followed by depositing another atomic layer of Cu metal, and replacement with Pt^{4+} resulting in a Pd film with the surface modified by Pt. Figure 2.3 displays the current-potential-time trace for the Pd cycle, where Cu UPD is followed by Pd replacement. The Cu^{2+} solution was introduced to the cell at a flow rate of 17 mL/min for 18 sec, at 0.15V, to form the sacrificial UPD Cu layer. This was followed by introduction of the Pd^{2+} solution, at open circuit, allowing Pd to replace the Cu UPD layer. The potential increased during the replacement reaction, until it reached the programmed stop potential of 390 mV. The stop potential was chosen to prevent Pd oxidation. Reaching the stop potential triggered a blank rinse with flowing 0.1 M H_2SO_4 at open-circuit potential (OCP). The cycle was then repeated a sufficient number of times to produce the desired deposit thickness.

Surface modification with Pt was achieved similarly. Cu UPD layer was first deposited, followed by introduction of Pt^{4+} ions at open circuit. The result was that each Pt^{4+} ion received two electrons from the equivalent of two UPD Cu atoms. The resulting

Pt coverage on the Pd surface was modified by either adjusting the Cu UPD potential, in order to deposit fractions of a monolayer, or by repeating the cycle to achieve Pt coverages slightly greater than a monolayer. For purposes limited to this paper, we define an amount of charge corresponding to one monolayer (ML) as 448 $\mu C/cm^2$ for a two electron process for the electrode area defined in our electrochemical cell. The stop potential was maintained at 390 mV to avoid oxidation of the underlying Pd layer. The Pd and Pt coverages were determined using the charge for Cu UPD, and the assumption of 100% exchange efficiency, so the coverages reported here are the maximum possible under the conditions used. The relationship between Pd coverage and the number of cycles is shown in Figure 2.4. In the present study, 5 cycles were grown, with each cycle depositing 0.5 ML, in order to produce a Pd coverage of 2.5 ML, as some reports suggest that Pd only starts absorbing hydrogen above 2 ML [20, 29, 30]. Pd nanofilm coverages were also determined by their oxidative stripping in 50 mM HCl, scanning from 150 mV to 700 mV. The linearity of the graph in Figure 2.4 is consistent with ALD and layer by layer growth, where doubling the cycles doubled the coverage.

Figure 2.5 displays a CV for a 2.5 ML Pd film in 0.1 M H_2SO_4 over the hydrogen sorption region. The scan was begun negatively from the OCP, reversed at -250 mV and ended at 150 mV. This range of potentials corresponds to where H sorption and desorption take place on Pd. The first reduction peak, -8 mV, indicates hydrogen adsorption, or the surface hydride peaks (UPD H) on Pd. The second broad peak at -200mV indicates hydrogen absorption into bulk Pd, and this was followed by

absorption convoluted with H_2 evolution near -250 mV. Sufficient absorption into the bulk results in the formation of the β-hydride (PdH_x) [31]. After reversal of the potential scan at -250 mV, hydrogen

desorption began, peaking near -200 mV. Desorption of the adsorbed layer of hydrogen atoms (H UPD) is peaked at 0 mV. The adsorption and absorption characteristically occur at different potentials on thin films. In similar CVs using thicker films or bulk Pd, surface hydride peaks are normally not observed because of the large currents for H absorption and its subsequent desorption, relative to H UPD [32].

Based on the CV in Figure 2.5, a potential sequence was designed to first saturate the Pd film with hydrogen at negative potential, followed by stepping the potential to 0 mV and using coulometry to determine how much hydrogen desorbed. Thus the films were initially equilibrated in 0.1 M H_2SO_4 at 150 mV for 10 s (point X) then stepped to -250 mV and held for 5 minutes (point Y). To determine the amount of absorbed hydrogen, the potential was stepped from -250 mV to 0 mV for 10 s, to strip the absorbed hydrogen (point Z).

Figure 2.6 is an example of the hydrogen oxidation current vs. time trace for a 2.5 ML Pd thin film. Integration of the current peak was used to determine the moles of hydrogen in the Pd film. The moles of Pd in the film were determined by summing the coulometry for Cu UPD from each Pd SLRR cycle used to form the film. H/Pd molar ratios at saturation have been reported to be between 0.6 to 0.8 [22, 24, 27, 31, 33-35]. We obtain values near 0.7 for the H/Pd ratio for our Pd films. Charges for hydrogen

oxidation were used rather than hydrogen absorption because it can be difficult to distinguish charge due to H_2 evolution from charge due to absorption.

Figure 2.7 displays the H/Pd ratio as a function of the amount of Pt modifying the Pd surface. There is essentially no significant effect observed on the H/Pd ratio as a function of the Pt coverage, in contrast to values reported in the literature for Pd-Pt alloys. For alloys, the capacity H/Pd ratio decreases rapidly with increasing amounts of Pt, almost completely losing its ability to store H for alloys with a Pt mole fraction above 19% [36-40].

Kinetics of hydrogen desorption: Figure 2.8 compares the hydrogen oxidation currents for unmodified and modified Pd films. It indicates that the presence of even 0.01 ML of Pt on the Pd surface causes a dramatic increase in the hydrogen oxidation current. In addition, the current decays to values close to zero much faster with Pt covering the surface, indicating that the hydrogen from the films desorbs much faster when Pt is on the surface.

Curve fits: Curve fits to the current for hydrogen oxidation were used to investigate changes in the mechanism of hydrogen desorption. A biexponential function, including an offset current (I_o) gave a good fit to the decay region of the current-vs.-time curves. The offset current might be attributable to background processes such as oxidation of aqueous H_2. A simple interpretation of the biexponential function is that there are two independent processes, such as absorption and adsorption, each with capacities C_1 and C_2 (mol H/mol Pd) within the film and each with a different first-order

rate constant, the reciprocal of which are the time constants t_1 and t_2. This can be expressed as:

$$I = I_0 + \frac{FAC_1 d}{Mt_1} e^{-t/t_1} + \frac{FAC_2 d}{Mt_2} e^{-t/t_2} \qquad \text{(Eq.1)}$$

where F is the Faraday constant (coulombs/mol), A is the electrode area (cm^2), d is the film thickness (cm), and M is the molar volume of palladium (cm^3/mol). The capacities C_1 and C_2 can be related to the ratio of the charge for hydrogen absorption and half the charge for Pd stripping. This number is also the molar H/Pd ratio.

A plot of the time constants versus the Pt coverage (Figure 2.9) shows that even a small amount of Pt on the surface results in an increase in the kinetics of the hydrogen oxidation reaction. For the coverages studied, the time constants dropped with increasing Pt coverage, plateauing near a ML. The presence of two time constants may indicate parallel processes for hydrogen desorption from Pd. It is possible that the hydrogen present within the crystal structure is desorbed quickly (characterized by t_1) and the second time constant (t_2) could be measuring desorption of H from at or near surfaces or grain boundaries, or from the dilute α phase. However, the time constants show a similar trend in their decrease with increasing Pt present on the surface indicating a faster desorption rate for each process.

Mechanism: Numerous theories have been presented regarding the mechanism of hydrogen absorption into Pd. Jerkiewicz et al. [41] describe an indirect mechanism for hydrogen absorption into Pd. According to that mechanism, the hydrogen is first adsorbed on the electrode surface (UPD H). The surface hydrogen moves into empty

subsurface sites, followed by diffusion into the bulk to form a non-stoichiometric compound (PdH_x).

Bartlett et al. [23] suggest a direct absorption of hydrogen into Pd that occurs in a single step:

$$H_3O^+ + e^- \rightarrow H_{abs} + H_2O \qquad \text{(Eq.2)}$$

They propose this based on their observation that UPD H peaks are greatly diminished in their voltammograms in the presence of surface Pt [23]. They suggest that the surface hydride acts as a spatial obstacle that blocks direct absorption.

The work presented here was undertaken in response to the theoretical work of Greeley and Mavrikakis [42], which supports the indirect mechanism. In that scenario, the surface hydride is destabilized in the presence of Pt, shifted to a potential near that for bulk absorption, or a distribution of potentials between the UPD peak and absorption peak. The destabilized surface hydride has a lower activation barrier to enter bulk states, leading to faster absorption and desorption rates.

Figure 2.10 shows a comparison between a CV of a 2.5 ML Pd film and a 2.5 ML Pd film modified with 0.1 ML Pt on its surface, in 0.1 M H_2SO_4. There is a clear reduction in the surface hydride peak at -8 mV when Pt is present. A prior report of E-ALD of a Pt multilayer film on Au [28] using similar conditions shows hydride peaks at +50 and -100 mV, and only for surfaces cleaned through oxidative cycles. This suggests that the surface hydrides on the Pd surface are modified into a distribution of stabilities in the presence of Pt, some of which are more or less stable than for pure Pd. Contaminants

adsorbed to the Pt may have some influence on surface hydride formation, but based on our observations, any such contaminants that are present do not inhibit transport of hydrogen between the electrode and solution.

It is not proposed here that the surface hydride is so destabilized in the presence of Pt that it is not present at all, as would be necessary to spatially unblock the direct pathway, described by Bartlett et al. [23]. If that were the case, it would not be possible to grow multiple cycles of Pt using the surface hydride as the sacrificial layer, as has been achieved by Vasiljevic et al [43] and this group. By that argument, the indirect mechanism is more consistent with reported observations. Another consideration described by Łukaszewski et al. [44] is that the transition from the solid solution (α phase) to the formation of the non-stoichiometric compound (β phase) involves rearrangement of Pd atoms, and not just hydrogen atoms. If the rearrangement of Pd atoms is slow, this could be the rate-limiting step, instead of transport of hydrogen from surface to bulk. The fact that various groups, in addition to this one, have observed strong effects from surface modification suggests that the Pd atom rearrangement is not the rate-limiting step, at least in the case of nanometer-scale films or porous structures.

Conclusions

When the surfaces of Pd nanofilms were modified with Pt, peak hydrogen oxidation currents increased, even with submonolayer amounts of Pt, indicating a catalytic effect on the reaction. Fits to a simple kinetic model showed enhancement of the oxidative hydrogen desorption rate for films coated with Pt by over an order of magnitude, though the enhancement was not greatly sensitive to the amount of Pt present

for coverages near a ML. The H/Pd ratio did not change significantly as a function of the amount of deposited Pt, suggesting it remained as a surface layer, and did not form an alloy.

When considered in the context of other recent work, the results described here support a mechanism in which hydrogen absorption and desorption are mediated by a surface hydride, and each process can be limited by desorption of the surface hydride into the aqueous or bulk solid phase. The presence of Pt on the surface destabilizes some of the surface hydride sites, accelerating hydrogen transport between surface and bulk. Proper understanding of this mechanism is likely to be important in the development of hydrogen storage and separation devices that use palladium, and perhaps other materials where surface species are important.

Acknowledgements

We acknowledge the support of the National Science Foundation, Division of Materials Research no. 1410109 and the Laboratory-Directed Research and Development program at Sandia National Laboratories, a multiprogram laboratory managed and operated by Sandia Corporation, a wholly owned subsidiary of Lockheed martin Corporation, for the U.S. Department of Energy's National Nuclear Security Administration under contract DE-AC04-94AL85000.

References

1. Crabtree, G.W., M.S. Dresselhaus, and M.V. Buchanan, *The hydrogen economy.* Physics Today, 2004. **57**(12): p. 39-44.
2. Bartlett, P.N., et al., *The preparation and characterisation of H1-e palladium films with a regular hexagonal nanostructure formed by electrochemical deposition from lyotropic liquid crystalline phases.* Physical Chemistry Chemical Physics, 2002. **4**(15): p. 3835-3842.
3. T B Flanagan, a. and W.A. Oates, *The Palladium-Hydrogen System.* Annual Review of Materials Science, 1991. **21**(1): p. 269-304.
4. Favier, F., et al., *Hydrogen sensors and switches from electrodeposited palladium mesowire arrays.* Science, 2001. **293**(5538): p. 2227-2231.
5. Antolini, E., *Palladium in fuel cell catalysis.* Energy & Environmental Science, 2009. **2**(9): p. 915-931.
6. Stickney, J.L., *Electrochemical atomic layer epitaxy (EC-ALE): Nanoscale control in the electrodeposition of compound semiconductors.* Advances in Electrochemical Science and Engineering, 2002. **7**: p. 1-106.

7. Cavallini, M., et al., *Two-dimensional self-organization of CdS ultra thin films by confined electrochemical atomic layer epitaxy growth.* The Journal of Physical Chemistry C, 2007. **111**(3): p. 1061-1064.

8. Gregory, B.W. and J.L. Stickney, *Electrochemical atomic layer epitaxy (ECALE).* Journal of Electroanalytical Chemistry and Interfacial Electrochemistry, 1991. **300**(1–2): p. 543-561.

9. Banga, D.O., et al., *Formation of PbTe nanofilms by electrochemical atomic layer deposition (ALD).* Electrochimica Acta, 2008. **53**(23): p. 6988-6994.

10. Wade, T.L., et al., *Electrodeposition of InAs.* Electrochemical and Solid-State Letters, 1999. **2**(12): p. 616-618.

11. Foresti, M.L., et al., *Electrochemical atomic layer epitaxy deposition of CdS on Ag (111): An electrochemical and STM investigation.* Journal of Physical Chemistry B, 1998. **102**(38): p. 7413-7420.

12. Boone, B.E. and C. Shannon, *Optical Properties of Ultrathin Electrodeposited CdS films Probed by Resonance Raman Spectroscopy and Photoluminescence.* Journal of Physical Chemistry, 1996. **100**(22): p. 9480-9484.

13. Mrozek, M.F., Y. Xie, and M.J. Weaver, *Surface-Enhanced Raman Scattering on Uniform Platinum-Group Overlayers: Preparation by Redox Replacement of Underpotential-Deposited Metals on Gold.* Analytical Chemistry, 2001. **73**(24): p. 5953-5960.

14. Vasilic, R. and N. Dimitrov, *Epitaxial Growth by Monolayer-Restricted Galvanic Displacement.* Electrochemical and Solid-State Letters, 2005. **8**(11): p. C173-C176.

15. Kim, Y.-G., et al., *Platinum Nanofilm Formation by EC-ALE via Redox Replacement of UPD Copper: Studies Using in-Situ Scanning Tunneling Microscopy.* The Journal of Physical Chemistry B, 2006. **110**(36): p. 17998-18006.

16. Gewirth, A.A. and B.K. Niece, *Electrochemical applications of in situ scanning probe microscopy.* Chem. Rev., 1997. **97**: p. 1129-1162.

17. Kibler, L.A., et al., *Initial stages of Pd deposition on Au(hkl) Part I: Pd on Au(111).* Surface Science, 1999. **443**(1–2): p. 19-30.

18. Brankovic, S.R., J.X. Wang, and R.R. Adžić, *Metal monolayer deposition by replacement of metal adlayers on electrode surfaces.* Surface Science, 2001. **474**(1–3): p. L173-L179.

19. Flanagan, T.B. and F.A. Lewis, *Hydrogen absorption by palladium in aqueous solution.* Transactions of the Faraday Society, 1959. **55**(0): p. 1400-1408.

20. Baldauf, M. and D.M. Kolb, *A hydrogen adsorption and absorption study with ultrathin Pd overlayers on Au(111) and Au(100).* Electrochimica Acta, 1993. **38**(15): p. 2145-2153.

21. Quaino, P., et al., *Theory meets experiment: Electrocatalysis of hydrogen oxidation/evolution at Pd–Au nanostructures.* Catalysis Today, 2011. **177**(1): p. 55-63.

22. Czerwiński, A., S. Zamponi, and R. Marassi, *The influence of carbon monoxide on hydrogen absorption by thin films of palladium.* Journal of Electroanalytical Chemistry and Interfacial Electrochemistry, 1991. **304**(1–2): p. 233-239.

23. Bartlett, P.N. and J. Marwan, *The effect of surface species on the rate of H sorption into nanostructured Pd.* Physical Chemistry Chemical Physics, 2004. **6**(11): p. 2895-2898.

24. Sheridan, L.B., et al., *Hydrogen sorption properties of bare and Rh-modified Pd nanofilms grown via surface limited redox replacement reactions.* Electrochimica Acta, 2014. **128**(0): p. 400-405.

25. Sheridan, L.B., et al., *Electrochemical Atomic Layer Deposition (E-ALD) of Palladium Nanofilms by Surface Limited Redox Replacement (SLRR), with EDTA Complexation.* Electrocatalysis, 2012. **3**(2): p. 96-107.

26. Sheridan, L.B., et al., *Formation of Palladium Nanofilms Using Electrochemical Atomic Layer Deposition (E-ALD) with Chloride Complexation.* Langmuir, 2013. **29**(5): p. 1592-1600.

27. Sheridan, L.B., et al., *Hydrogen Adsorption, Absorption, and Desorption at Palladium Nanofilms formed on Au(111) by Electrochemical Atomic Layer*

Deposition (E-ALD): Studies using Voltammetry and In Situ Scanning Tunneling Microscopy. Journal of Physical Chemistry C, 2013. **117**(30): p. 15728-15740.

28. Jayaraju, N., et al., *Electrochemical Atomic Layer Deposition (E-ALD) of Pt Nanofilms Using SLRR Cycles.* Journal of the Electrochemical Society, 2012. **159**(10): p. D616-D622.

29. Álvarez, B., et al., *Electrochemical properties of palladium adlayers on Pt(100) substrates.* Surface Science, 2004. **573**(1): p. 32-46.

30. Tang, J., et al., *Pd deposition onto Au(111) electrodes from sulphuric acid solution.* Electrochimica Acta, 2005. **51**(1): p. 125-132.

31. Bartlett, P., et al., *The preparation and characterisation of H 1-e palladium films with a regular hexagonal nanostructure formed by electrochemical deposition from lyotropic liquid crystalline phases.* Physical Chemistry Chemical Physics, 2002. **4**(15): p. 3835-3842.

32. Czerwiński, A., et al., *The study of hydrogen sorption in palladium limited volume electrodes (Pd-LVE): I. Acidic solutions.* Journal of Electroanalytical Chemistry, 1999. **471**(2): p. 190-195.

33. Rafizadeh, H.A., *Lattice dynamics of metal hydrides.* Physical Review B, 1981. **23**(4): p. 1628-1632.

34. Gabrielli, C., et al., *Investigation of Hydrogen Adsorption and Absorption in Palladium Thin Films: II. Cyclic Voltammetry.* Journal of The Electrochemical Society, 2004. **151**(11): p. A1937-A1942.

35. Stickney, J.L., L. Sheridan, and D. Robinson, *Pd nanofilm formation on Au single crystal substrates, using electrochemical ALD.* Abstracts of Papers of the American Chemical Society, 2012. **244**.

36. Grden, M., et al., *Hydrogen electrosorption in Pd-Pt alloys.* Journal of Electroanalytical Chemistry, 2002. **532**(1-2): p. 35-42.

37. Łukaszewski, M., M. Grdeń, and A. Czerwiński, *Comparative study on hydrogen electrosorption in palladium and palladium-noble metal alloys.* Journal of New Materials for Electrochemical Systems, 2006. **9**: p. 409-417.

38. Lukaszewski, M., K. Hubkowska, and A. Czerwinski, *Electrochemical absorption and oxidation of hydrogen on palladium alloys with platinum, gold and rhodium.* Physical Chemistry Chemical Physics, 2010. **12**(43): p. 14567-14572.

39. Łukaszewski, M., et al., *Correlations between hydrogen electrosorption properties and composition of Pd-noble metal alloys.* Electrochemistry Communications, 2007. **9**(4): p. 671-676.

40. Moysan, I., et al., *Pd–Pt alloys: correlation between electronic structure and hydrogenation properties.* Journal of Alloys and Compounds, 2001. **322**(1–2): p. 14-20.

41. Jerkiewicz, G. and A. Zolfaghari, *Comparison of hydrogen electroadsorption from the electrolyte with hydrogen adsorption from the gas phase.* Journal of the Electrochemical Society, 1996. **143**(4): p. 1240-1248.

42. Greeley, J. and M. Mavrikakis, *Surface and subsurface hydrogen: Adsorption properties on transition metals and near-surface alloys.* The Journal of Physical Chemistry B, 2005. **109**(8): p. 3460-3471.

43. Nutariya, J., et al., *Growth of Pt by surface limited redox replacement of underpotentially deposited hydrogen.* Electrochimica Acta, 2013. **112**(0): p. 813-823.

44. Lukaszewski, M., et al., *Kinetics and mechanism of hydrogen electrosorption in palladium-based alloys.* Solid State Ionics, 2011. **190**(1): p. 18-24.

Figures

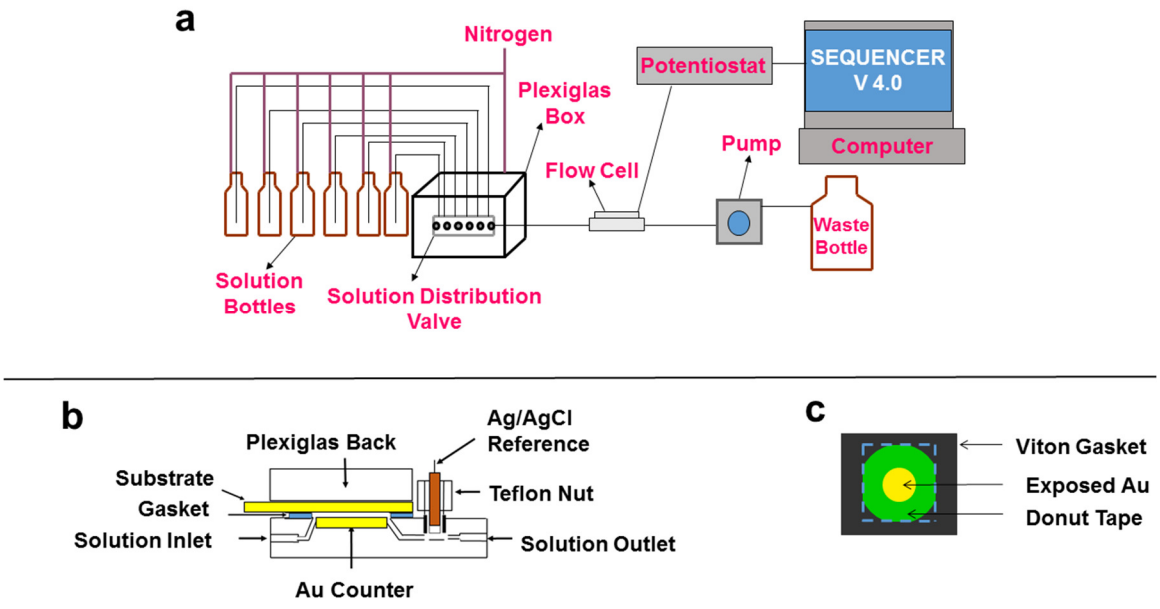

Figure 2.1: (a) Schematic representation of an E-ALD flow cell system, (b) Lateral view of flow cell, (c) Top view of gold slide.

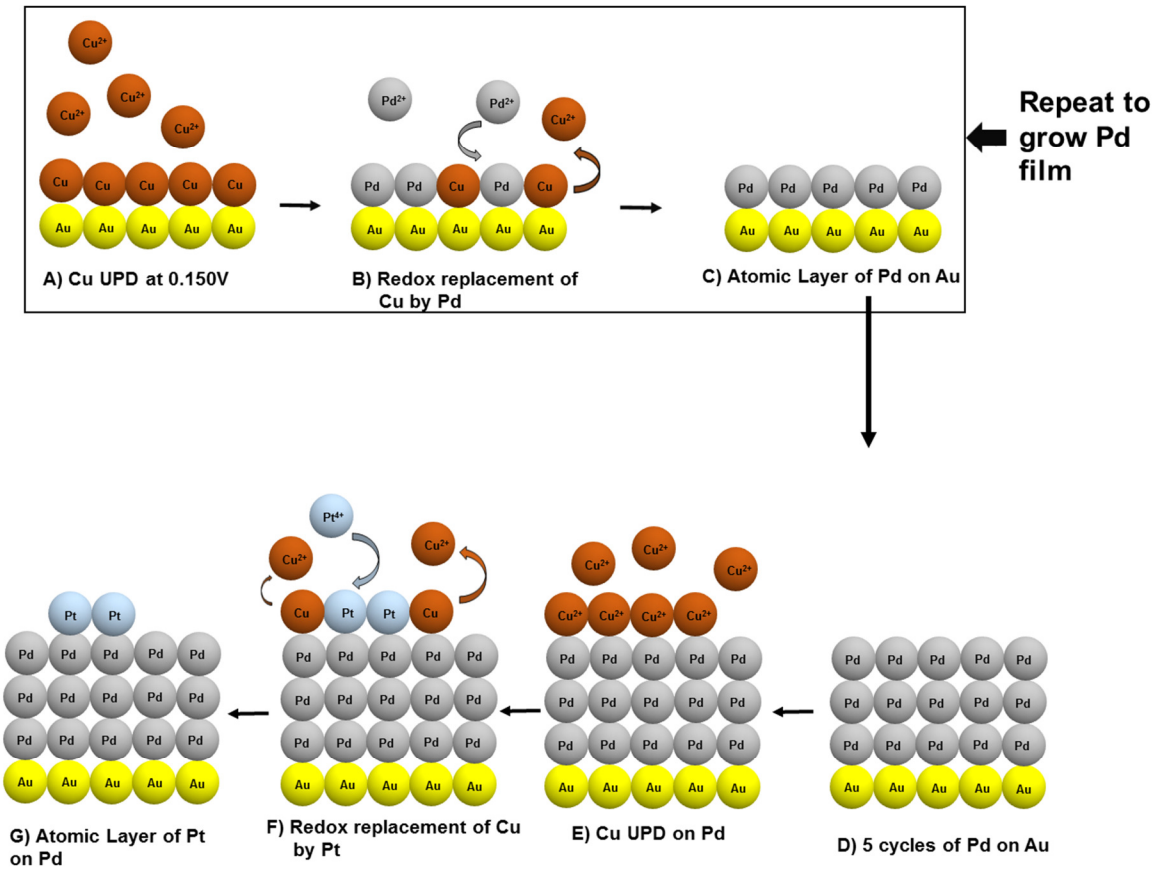

Figure 2.2: Schematic of E-ALD SLRR cycles for Pd and Pt

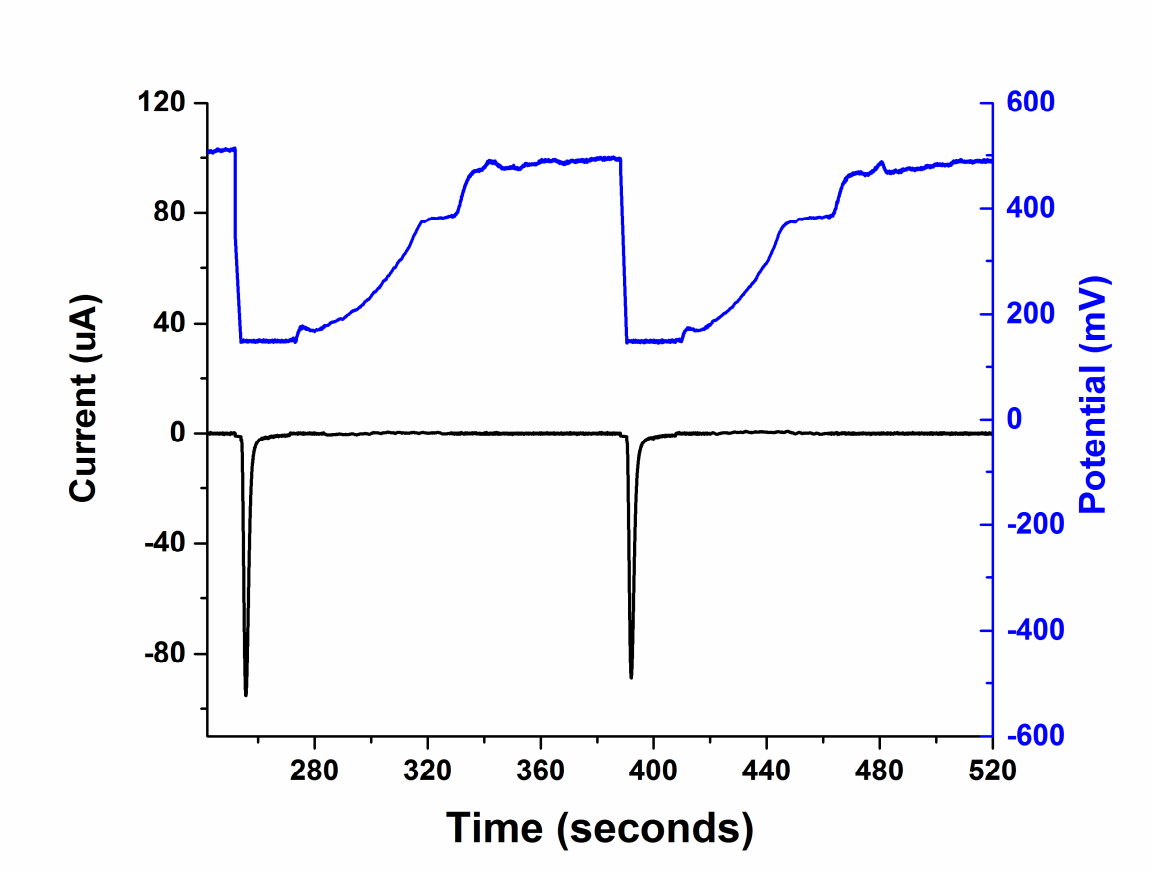

Figure 2.3: Current-Potential-Time trace illustrating the Pd E-ALD cycles

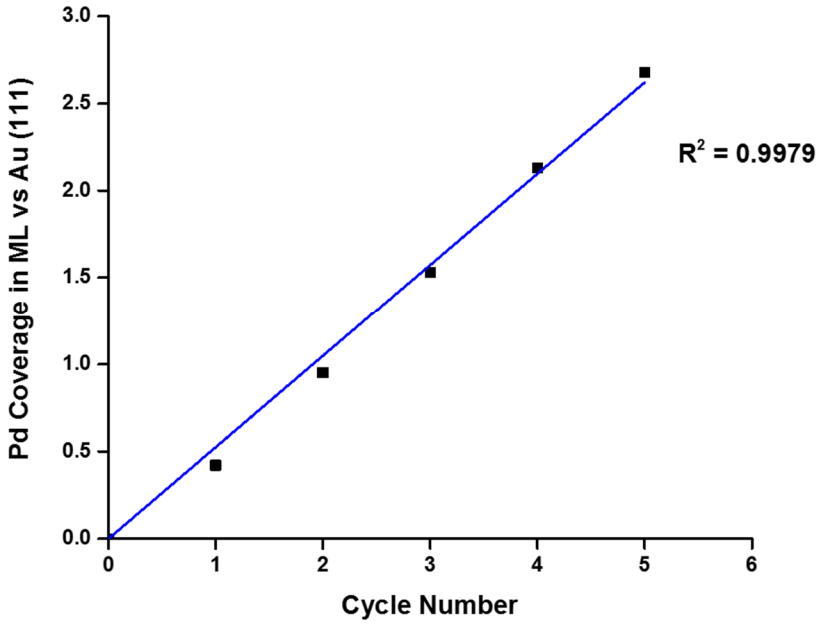

Figure 2.4: Plot of Pd coverage vs. the number of cycles performed

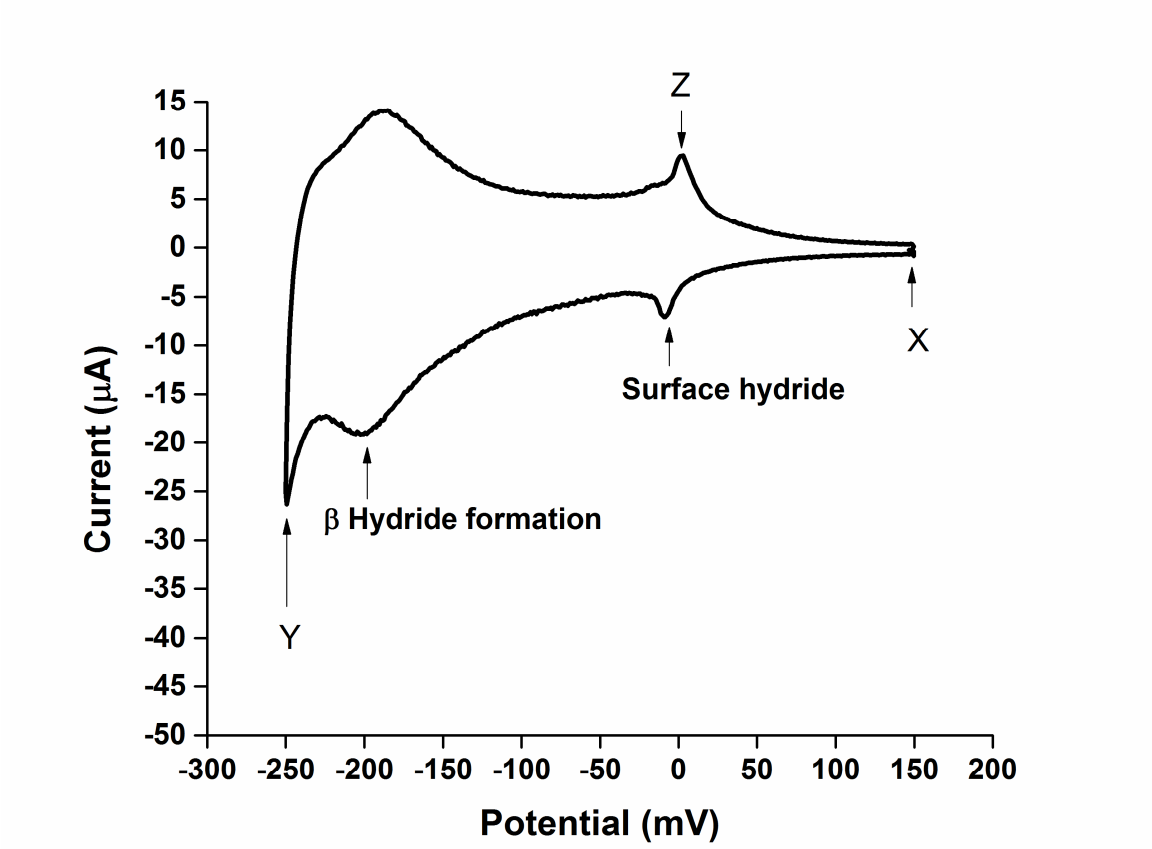

Figure 2.5: CV of 2.5 ML Pd nano-film in 0.1M H_2SO_4, performed at 10 mV/s. Potentials for charging and discharging the film with hydrogen, indicated by X, Y and Z, are discussed in text below.

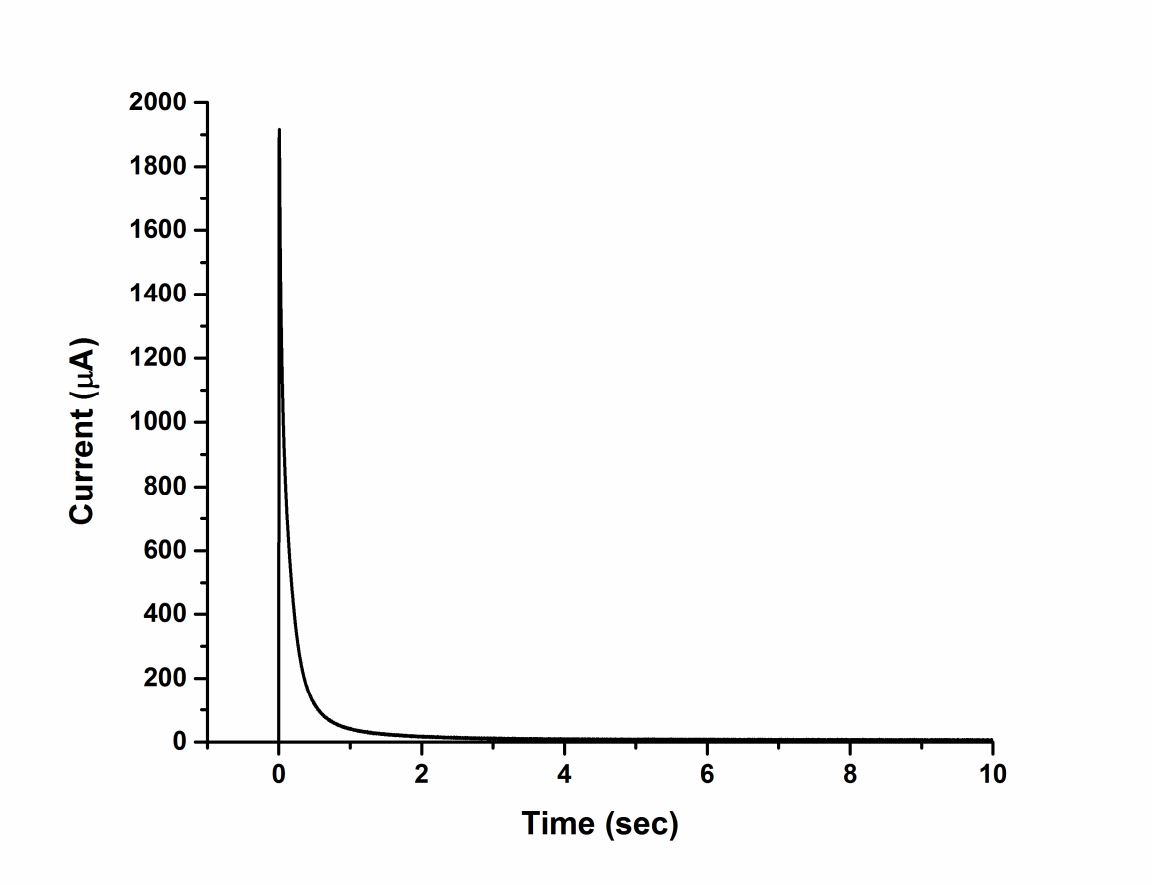

Figure 2.6: Hydrogen oxidation current vs. time trace for a 2.5 ML thin film saturated with hydrogen, on stepping from -250 mV to 0 mV

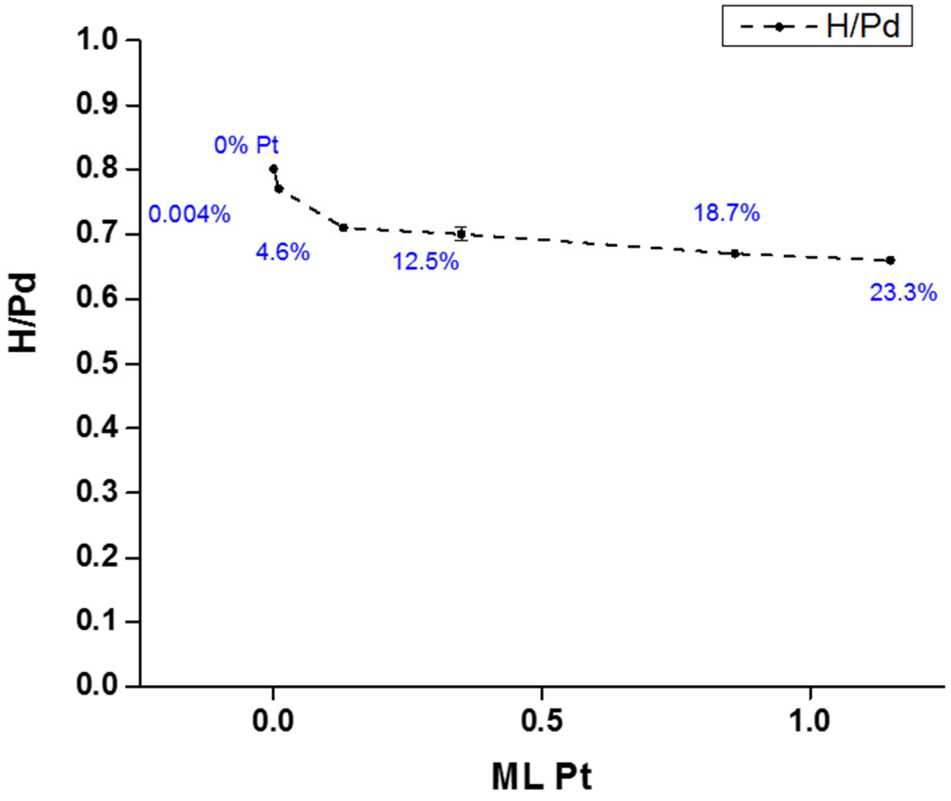

Figure 2.7: H/Pd ratio with increasing Pt coverage with Pt coverage shown as % within the figure

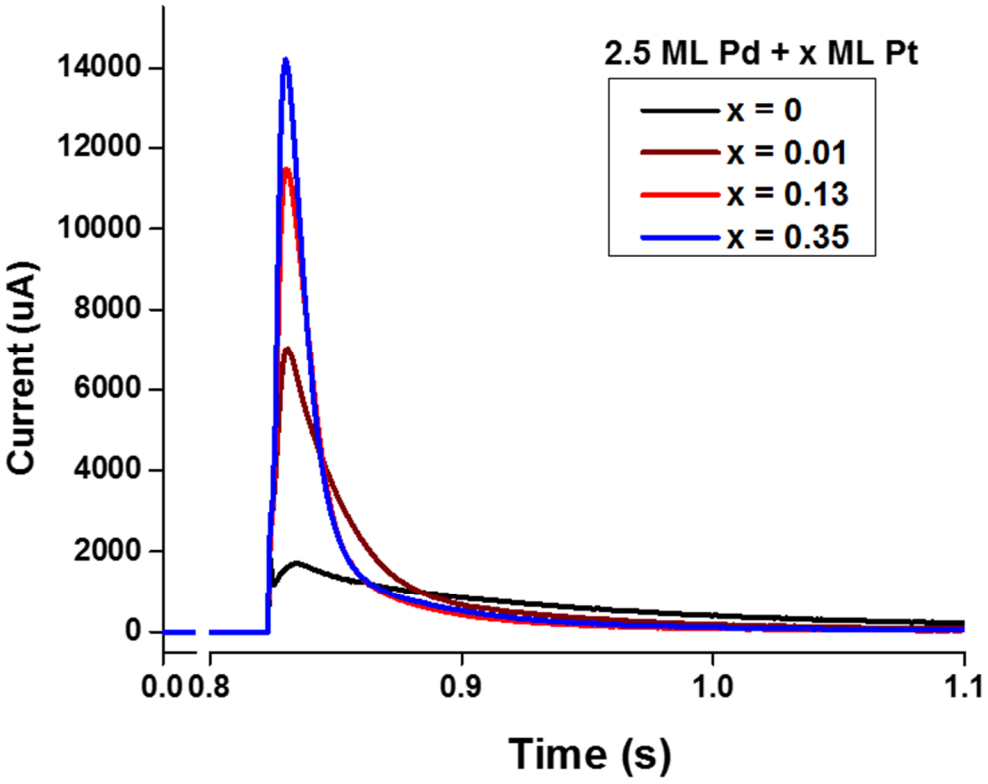

Figure 2.8: Comparison of H oxidation currents for Pd and Pt modified Pd films

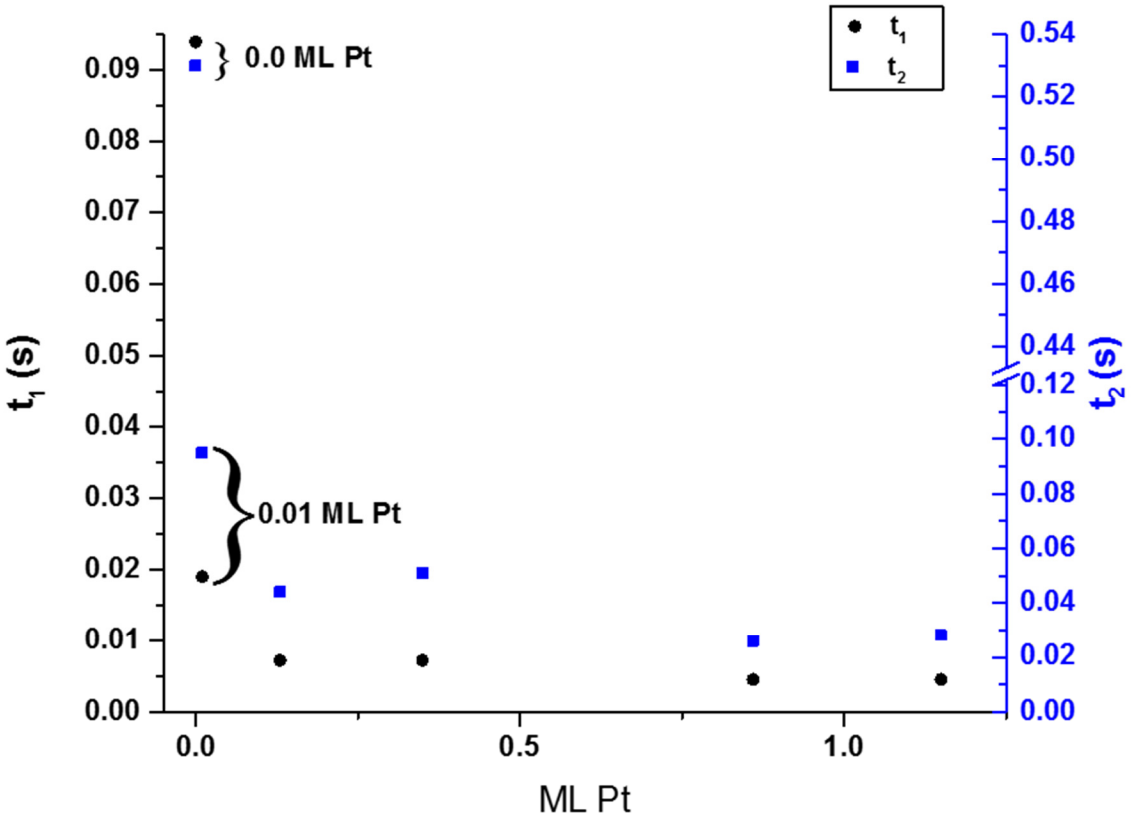

Figure 2.9: Decay constants for desorption of hydrogen from bare 2.5 ML Pd and Pt modified Pd thin films

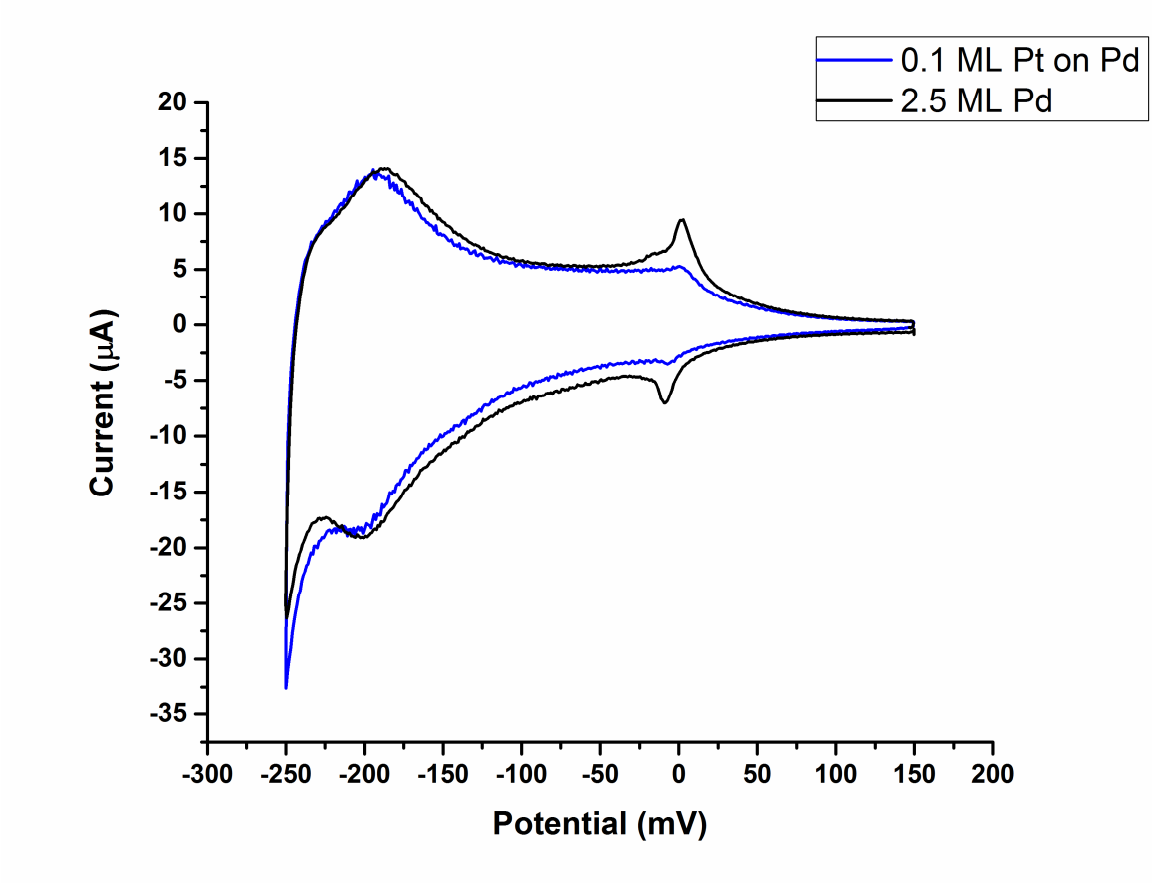

Figure 2.10: CVs of 2.5 ML Pd nano-film (black line) and 2.5 ML Pd film modified with 0.1 ML Pt on the surface (blue line) in 0.1 M H_2SO_4, performed at 10 mV/s. Note the reduction in surface hydride when Pt is present on the surface.

CHAPTER 3

ELECTROLESS ATOMIC LAYER DEPOSITION (EL-ALD) OF PALLADIUM

---

[1]Kaushik Jagannathan, Victoria Pham, Sheng Shen, John L. Stickney, To be submitted to *Journal of the Electrochemical Society*

Introduction

Electroless deposition is a technique where materials are deposited without an external current source. Just as in electrodeposition, the quality of the deposit depends on the reaction conditions and the morphology and composition of the substrate. However, the difference lies in the ability to deposit on not just conductive substrates like metals but also on semi conductive substrates (FTO, ITO) and non-conductive substrates (glass)

Pd has a wide variety of applications in fields such as fuel cells [1-7] and sensors [8-16]. Typically, Pd has been electrodeposited by various techniques such as sputter deposition [17-19], chemical vapor deposition [20-22] and electrodeposition [23-27]. However, electroless deposition of Pd is also possible. In general, electroless deposition of metal and alloys involves a cathodic reduction of the metal ions and requires the presence of oxidizing agents as part of the electrolyte. One method of electroless deposition is by a two-step process [28]. The first step involves a sensitization process by adsorption of Sn^{2+} ions from solution. This is followed by an activation process by introducing Pd^{2+} ions. The adsorbed Sn^{2+} ions are oxidized to Sn^{4+} by the Pd^{2+} ions, which in turn reduce to Pd^{0}. Variations of the technique have been patented [28, 29]. Horkans has studied activation by Sn-Pd colloidal catalysts in a single step using cyclic voltammetry and reported that the adsorption of Sn occurs in clumps [30]. Kim et al. also report much higher activation times for the two step process compared to the single step process [31]. Cohen and West studied $SnCl_2.2H_2O$ solutions by Mosbauerr spectroscopy and reported the presence of Sn^{4+} ions from dissolved and atmospheric oxygen [32].

Meek investigated Pd-Sn colloids and reported that the order of mixing the components of the Sn solution had an effect on the size of the particles [33].

It is also possible to use the activated Pd as a catalyst to deposit other metals. For example, Hsu et al. have carried out electroless deposition of Cu seed layer on Sn-Pd treated TaN diffusion barrier layers [34]. The present chapter describes the use of the Sn-Pd treatment for controlled electroless atomic layer deposition of Pd (EL-ALD). Electroless atomic layer deposition (E-ALD) of Pd on polycrystalline and single crystal Au has been studied by the author's group [35-38]. This chapter describes an electroless atomic layer deposition (EL-ALD) sequence that has been developed to grow Pd monolayers on FTO, ITO, Au and glass. The deposits were investigated by coulometry, atomic force microscopy (AFM) and scanning electron microscopy (SEM). Preliminary results are discussed regarding growth mechanisms, deposit quality and possible improvements to the technique. Initial studies indicate a layer by layer growth similar to an E-ALD process.

Experimental

Substrates included Vapor deposited Au on glass slides (100 nm Au on a 5 nm Ti adhesion layer, EMF Corporation), Fluorine doped tin oxide (FTO**),** Tin doped indium oxide (ITO), (R_s = 70-100 Ohms, Delta Technologies Limited) and glass (Gold Seal). Prior to deposition, the FTO and ITO samples were subjected to sequential sonication in acetone for 20 minutes, 18 MΩ-cm ultrapure water (Milli-Q Advantage A10), and

acetone. Solutions were prepared with 18 MΩ-cm ultrapure water (Milli-Q Advantage A10). The Pd solution was 0.1 mM ultrapure-grade $PdCl_2$ (Aldrich Chemicals) in 50 mM HCl, in which the tetrachloropalladate ion $PdCl_4^{2-}$ is expected to form. The Cu solution used for E-ALD was 1 mM $CuSO_4$ (J.T. Baker Chemical Co., 99.8%) and 0.1 M H_2SO_4. Sn solution consisted of 1 mM and 10 mM $SnCl_2$ (J.T. Baker Chemical Co., 98.8%) in 0.1 M HCl, forming Sn^{2+} ions. The deposits were grown and studied in an automated electrochemical flow deposition system (Electrochemical ALD L.C., Athens, GA), diagramed in Figure 3.1. The system consisted of five solution reservoirs, 5 valves and a variable speed peristaltic pump. The valves were housed in a Plexiglas box along with the solution reservoirs so they could be purged continuously with N_2, to minimize exposure to O_2. The electrochemical flow cell, downstream from the valves, was also made of Plexiglas and had a volume of around 0.15 mL. A three electrode cell configuration was used, with a gold wire auxiliary electrode embedded in the front cell plate, directly across from the substrate. The reference was an Ag/AgCl electrode (3 M KCl) from Bioanalytical systems, against which potentials have been reported. E-ALD software "Sequencer-4" was used to control valves, pump and potentials.

AFM imaging was carried out in air via intermittent contact mode (Molecular Imaging, Pico Plus). Samples were analyzed using AFM image analysis software (PicoView, v 1.14.3) to determine the effect of sample number on particle distribution on the glass substrates. Additionally, Scanning Electron Microscopy (SEM) imaging was performed with a FEI Inspect F FEG-SEM on ITO substrates.

Results and Discussions

Growth of EL-ALD nanofilms: Prior to deposition, all three types of substrates were cleaned by cycling in 0.1 M H_2SO_4 by scanning from -200 mV to 1400 mV at 10 mV/s. Figure 3.1 describes the electroless deposition of Pd films by a two-step sensitization and activation process. All the steps indicated below are at open circuit potential (OCP). First, Sn^{2+} ions are introduced into the flow cell at 17 mV/s by flowing for 30s. The pump is then turned off and the Sn^{2+} ions are adsorbed for 5 minutes. The excess or weakly adsorbed Sn^{2+} are rinsed out by flushing in 0.1 M H_2SO_4 at 17 mV/s for different times ranging from 30 s to 5 minutes. 3 minutes of rinsing was found to be sufficient based on the results (discussed below). Following the rinse step, Pd^{2+} ions are introduced by pumping for 15 seconds at 17 mV/s and then the pump is stopped to allow a surface limited redox replacement (SLRR) process to occur. The Pd^{2+} is reduced to Pd^0 by taking 2 electrons from the Sn^{2+} which in turn gets oxidized to Sn^{4+}. After 2 minutes of SLRR, a blank rinse step is initiated and the Sn^{4+} is then rinsed out of the cell by flowing in 0.1 M H_2SO_4 for 1 minute at 17 mV/s.

Film Characterization: Figure 3.2 shows the oxidation of the adsorbed Sn^{2+}, from a 10 mM solution, in 0.1 M H_2SO_4 at 10 mV/s. The oxidation potential shifts slightly indicating a small variability in the surface structure of the FTO. However, the peak currents are fairly constant for a 3 minute and a 5 minute rinse. Hence the EL-ALD sequence was designed with a 3 minute rinse. The amount of Sn^{2+} present was quantified by stepping from OCP to 1400 mV and measuring the resultant oxidation charge. Figure

3.3 shows a plot of the oxidation charges obtained for oxidation of Sn^{2+} adsorbed from a 10 mM solution and the OCP prior to oxidation as a function of rinse time. The oxidation charge for the 3 and 5 minute rinse times were lower than that of the 1 minute rinse, indicating that some Sn^{2+} was possibly weakly adsorbed. However, a slight variability in the amount of Sn ions adsorbed is present based on the small shift in oxidation potentials. In order to check the effect of concentration of the $SnCl_2$ on the amount of ions adsorbed, the experiment was repeated with a 1 mM $SnCl_2$ in 0.1 M HCl solution and 3 minutes of rinsing. As expected, a lower oxidation charge was obtained (87 μC) for the same rinse times (not shown in figure). Since the charges for the 3 minute and 5 minute rinse were similar, and adsorption time of 3 minutes was chosen. It is essential to determine the time needed to rinse the Sn ions since various groups have reported on the presence of any Sn ions having a negative effect on the activity after Pd sensitization [39, 40]. The concentration of the Sn solution used was maintained at 10 mM $SnCl_2$ and 0.1 M HCl.

Figure 3.4 is a plot of the OCP against time for the adsorption of Sn on FTO. As the solution is introduced into the cell, the potential drops rapidly and then gradually rises to 25 mV as the Sn^{2+} adsorption occurs. On rinsing, there is a more rapid increase in potential to 222 mV corresponding to removal of the excess ions that are not adsorbed or weakly adsorbed. Figure 3.5 is a plot of the OCP against time for the SLRR of Sn by Pd. On introducing the Pd there is a small dip in the potential to 192 mV as the solution in the cell is replaced, following which there is a rise in the potential to 255 mV as Pd ions are

flowed into the cell. As the SLRR proceeds, the potential rapidly rises to 353 mV indicating a replacement of Sn by Pd.

In order to calculate the amount of Pd deposited, the Pd deposit was stripped by scanning from 150 mV to 700 mV in 50 mM HCl at 5 mV/s. Multiple EL-ALD cycles of Pd deposition were carried out and stripped and the charges for stripping were plotted as a function of cycle number (Figure 3.6). The linearity indicates that the same amount of Pd is deposited from cycle to cycle. EL-ALD cycles of Pd on Au were also executed using the sequence described above.

Additionally, multiple cycles of Pd on deposition on Au slides by E-ALD were carried out by a previously optimized process [35, 36]. The deposits were again stripped in 50 mM HCl in a similar manner. The charges from stripping were converted to monolayers (ML). Figure 3.7 plots the Pd coverage from an E-ALD process against an EL-ALD process against the number of cycles. The linearity is common for both techniques indicating that both processes have a layer by layer growth mechanism on Au substrates. However, the coverage for the electroless process is almost three times less than for electrodeposition. This could be attributed to the fundamental mechanism of each process. In electrodeposition, the Cu is deposited at a controlled potential leading to more sacrificial metal atoms depositing than in an electroless process where the Sn ions are adsorbed at open circuit. Since the Pd replaces the Cu and Sn atoms, the amount of Pd deposited is a lot lesser in the latter technique.

AFM Imaging: AFM was carried out on Pd deposited from a 1 mM Sn solution on glass substrates. Figure 3.8 (a) is a blank glass slide with no deposition. Figure 3.8 (b) and (c) correspond to 5 and 10 cycles of Sn-Pd deposition from a 1 mM Sn

solution respectively. From the figure there is a clear indication that there are small islands of deposition formed which are absent on bare glass. The 10 cycle deposit shows an increase in the number of islands over the 5 cycle deposit for the same sample area. At the same time, the size of the islands is an indication of certain favored areas of deposition present which increase in size with an increase in deposition cycle.

Cu electrodeposition on Transparent Conducting Oxides: Cu electrodeposition was carried out on the TCO substrates for potential use in seed layers. Figure 3.9 is a cyclic voltammogram (CV) of a FTO glass slide in 1 mM $CuSO_4$ and 0.1 M H_2SO_4 at a scan rate of 10 mV/s. On scanning negative, there is a hysteresis loop present at 0 mV which is where bulk deposition of Cu occurs indicating nucleation and growth. On reversing the direction and scanning positive, there is a desorption peak at 30 mV. Figure 3.10 is a CV of an ITO glass slide in the same Cu solution and scan rate. There is again a hysteresis loop present at 0 mV and an oxidation peak slightly further positive at 70 mV/s on scanning positive. The charge for Cu reduction and oxidation is significantly higher on the ITO substrates, indicating that it is easier to deposit Cu on ITO.

In order to replicate the deposition schemes present in literature [41], the sequence for sensitization by Sn was slightly modified by removing the 3 minute rinse step after Sn adsorption. The activation process was unchanged. Following this, Cu solution was introduced into the cell at open circuit and then a potential step to -266 mV was applied for 10 seconds. The process was carried out on ITO substrates sensitized with a 1 mM and a 10 mM $SnCl_2$ and 0.1 M HCl solution. For a control experiment, Cu was directly electrodeposited on ITO. Figure 3.11 shows SEM images following Cu electrodeposition. Figure 3.11 (a) shows a blank ITO slide with no features present. 3.11

(b) shows Cu electrodeposited on to ITO without any sensitization and activation treatment. There is an even distribution of Cu nuclei on the ITO. However, when Cu is deposited on a substrate sensitized with 10 mM Sn solution and activated with Pd (3.11 (c)), the deposit shows some ring like structures which are larger than the nuclei obtained in the earlier case. On lowering the Sn concentration (3.11(d)) the nucleation density significantly lower, indicating that the interaction between the Cu and the substrate is somehow reduced. One possible reason could be the very high currents that are obtained by stepping to such a negative potential for Cu deposition. It is possible that the currents obtained could result in stripping the deposit or the underlying ITO layer. The CVs shown earlier clearly indicate that the process can occur much further positive than the potentials applied for this experiment. Another way of controlling the nucleation size could be the addition of solution containing the ammonate group as indicated by Osaka et al. [42].

Conclusions

The electroless deposition of Pd using a two-step process was investigated using cyclic voltammetry and microscopy. Initial results suggest a slight variability in the surface of the TCO electrodes. A linear relationship was obtained for multiple deposition cycles of Pd, indicating the process involves deposition of the same amount of Pd in each EL-ALD cycle. AFM indicates the formation of islands of Pd which grow with increasing deposition cycles. SEM of the deposits shows some unexpected features. One possible reason could be an unfavorable effect the high currents for Cu electrodeposition

have on the substrate. Schlesinger et al. found a non-linear relationship between the amount of Sn ions adsorbed and the metal islands formed per unit substrate area [43].

Future work would involve investigating the deposition process by growing thicker deposits. Hydrogen absorption and desorption into and out of the Pd can be used to study the coverage of Pd. Osaka et al. have added various accelerator solutions and found that these can affect the particle size and density [42]. Minjer and Boom reported that a treatment with $AgNO_3$ reduced the density of the Pd particles [44]. Based on these observations, it might be necessary to add and additional step after the activation step in order to get more homogenous and smaller sized particles. In addition, the stability of the ITO in the electrolytes needs to be investigated further. Preliminary investigations indicate the formation of nucleation sites. Studies on the effect of the size of these nuclei on the formation of thicker deposits will need to be investigated.

References

1. Antolini, E., *Palladium in fuel cell catalysis.* Energy & Environmental Science, 2009. **2**(9): p. 915-931.
2. Bianchini, C. and P.K. Shen, *Palladium-based electrocatalysts for alcohol oxidation in half cells and in direct alcohol fuel cells.* Chemical Reviews, 2009. **109**(9): p. 4183-4206.
3. Serov, A.A., et al., *Modification of palladium-based catalysts by chalcogenes for direct methanol fuel cells.* Electrochemistry communications, 2007. **9**(8): p. 2041-2044.
4. Xu, C., et al., *Highly ordered Pd nanowire arrays as effective electrocatalysts for ethanol oxidation in direct alcohol fuel cells.* Advanced Materials, 2007. **19**(23): p. 4256-4259.
5. Larsen, R., et al., *Unusually active palladium-based catalysts for the electrooxidation of formic acid.* Journal of Power Sources, 2006. **157**(1): p. 78-84.
6. Simões, M., S. Baranton, and C. Coutanceau, *Electro-oxidation of glycerol at Pd based nano-catalysts for an application in alkaline fuel cells for chemicals and energy cogeneration.* Applied Catalysis B: Environmental, 2010. **93**(3): p. 354-362.
7. Stahl, S.S., *Palladium-catalyzed oxidation of organic chemicals with O2.* Science, 2005. **309**(5742): p. 1824-1826.

8. Kim, K.T., S.J. Sim, and S.M. Cho, *Hydrogen gas sensor using Pd nanowires electro-deposited into anodized alumina template.* Sensors Journal, IEEE, 2006. **6**(3): p. 509-513.

9. Ding, D. and Z. Chen, *A Pyrolytic, Carbon-Stabilized, Nanoporous Pd Film for Wide-Range H2 Sensing.* Advanced Materials, 2007. **19**(15): p. 1996-1999.

10. Jakubik, W., M. Urbańczyk, and E. Maciak, *Metal-free phthalocyanine and palladium sensor structure with a polyethylene membrane for hydrogen detection in SAW systems.* Sensors and Actuators B: Chemical, 2007. **127**(1): p. 295-303.

11. Mubeen, S., et al., *Palladium nanoparticles decorated single-walled carbon nanotube hydrogen sensor.* The Journal of Physical Chemistry C, 2007. **111**(17): p. 6321-6327.

12. Tobiška, P., et al., *An integrated optic hydrogen sensor based on SPR on palladium.* Sensors and Actuators B: Chemical, 2001. **74**(1): p. 168-172.

13. Walter, E., F. Favier, and R. Penner, *Palladium mesowire arrays for fast hydrogen sensors and hydrogen-actuated switches.* Analytical chemistry, 2002. **74**(7): p. 1546-1553.

14. Atashbar, M.Z., D. Banerji, and S. Singamaneni, *Room-temperature hydrogen sensor based on palladium nanowires.* Sensors Journal, IEEE, 2005. **5**(5): p. 792-797.

15. Tien, C.-L., et al., *Hydrogen sensor based on side-polished fiber Bragg gratings coated with thin palladium film.* Thin Solid Films, 2008. **516**(16): p. 5360-5363.

16. Favier, F., et al., *Hydrogen sensors and switches from electrodeposited palladium mesowire arrays.* Science, 2001. **293**(5538): p. 2227-2231.

17. Jayaraman, V., et al., *Fabrication of ultrathin metallic membranes on ceramic supports by sputter deposition.* Journal of membrane science, 1995. **99**(1): p. 89-100.

18. RaviPrakash, J., et al., *Hydrogen sensors: Role of palladium thin film morphology.* Sensors and Actuators B: Chemical, 2007. **120**(2): p. 439-446.

19. Kreider, K.G., M.J. Tarlov, and J.P. Cline, *Sputtered thin-film pH electrodes of platinum, palladium, ruthenium, and iridium oxides.* Sensors and Actuators B: Chemical, 1995. **28**(3): p. 167-172.

20. Xomeritakis, G. and Y. Lin, *Fabrication of a thin palladium membrane supported in a porous ceramic substrate by chemical vapor deposition.* Journal of Membrane Science, 1996. **120**(2): p. 261-272.

21. Bhaskaran, V., M.J. Hampden-Smith, and T.T. Kodas, *Palladium Thin Films Grown by CVD from (1, 1, 1, 5, 5, 5-Hexafluoro-2, 4-pentanedionato) Palladium (II).* Chemical Vapor Deposition, 1997. **3**(2): p. 85-90.

22. Itoh, N., T. Akiha, and T. Sato, *Preparation of thin palladium composite membrane tube by a CVD technique and its hydrogen permselectivity.* Catalysis today, 2005. **104**(2): p. 231-237.

23. Baldauf, M. and D.M. Kolb, *A hydrogen adsorption and absorption study with ultrathin Pd overlayers on Au(111) and Au(100).* Electrochimica Acta, 1993. **38**(15): p. 2145-2153.

24. Brankovic, S., J. Wang, and R. Adžić, *Metal monolayer deposition by replacement of metal adlayers on electrode surfaces.* Surface Science, 2001. **474**(1): p. L173-L179.

25. Duncan, H. and A. Lasia, *Mechanism of hydrogen adsorption/absorption at thin Pd layers on Au(111).* Electrochimica Acta, 2007. **52**(21): p. 6195-6205.

26. Quaino, P. and E. Santos, *Hydrogen Evolution Reaction on Palladium Multilayers Deposited on Au (111): A Theoretical Approach.* Langmuir, 2015. **31**(2): p. 858-867.

27. Tang, J., et al., *Pd deposition onto Au(111) electrodes from sulphuric acid solution.* Electrochimica Acta, 2005. **51**(1): p. 125-132.

28. Shipley, J.C.R., *Method of electroless deposition on a substrate and catalyst solution therefor*. U.S. Patent 3011920, 1961

29. D'Ottavio, E.D., *Colloidal metal activating solutions for use in chemically plating nonconductors, and process of preparing such solutions*. U.S. Patent 3650913, 1970

30. Horkans, J., *A Cyclic Voltammetric Study of Pd-Sn Colloidal Catalysts for Electroless Deposition.* Journal of The Electrochemical Society, 1983. **130**(2): p. 311-317.

31. Kim, J.J. and S.H. Cha, *Optimized surface treatment of indium tin oxide (ITO) for copper electroless plating.* Japanese Journal of Applied Physics, 2002. **41**(11A): p. L1269.

32. Cohen, R. and K. West, *Solution chemistry and colloid formation in the tin chloride sensitizing process.* Journal of The Electrochemical Society, 1972. **119**(4): p. 433-438.

33. Meek, R., *A Rutherford Scattering Study of Catalyst Systems for Electroless Cu Plating II. Sensitization and Activation.* Journal of The Electrochemical Society, 1975. **122**(11): p. 1478-1481.

34. Hsu, H.-H., et al., *Sn/Pd catalyzation and electroless Cu deposition on TaN diffusion barrier layers.* Journal of The Electrochemical Society, 2002. **149**(3): p. C143-C149.

35. Sheridan, L.B., et al., *Electrochemical Atomic Layer Deposition (E-ALD) of Palladium Nanofilms by Surface Limited Redox Replacement (SLRR), with EDTA Complexation.* Electrocatalysis, 2012. **3**(2): p. 96-107.

36. Sheridan, L.B., et al., *Formation of Palladium Nanofilms Using Electrochemical Atomic Layer Deposition (E-ALD) with Chloride Complexation.* Langmuir, 2013. **29**(5): p. 1592-1600.

37. Sheridan, L.B., et al., *Hydrogen Adsorption, Absorption, and Desorption at Palladium Nanofilms formed on Au(111) by Electrochemical Atomic Layer*

Deposition (E-ALD): Studies using Voltammetry and In Situ Scanning Tunneling Microscopy. Journal of Physical Chemistry C, 2013. **117**(30): p. 15728-15740.

38. Stickney, J.L., L. Sheridan, and D. Robinson, *Pd nanofilm formation on Au single crystal substrates, using electrochemical ALD.* Abstracts of Papers of the American Chemical Society, 2012. **244**.

39. Gawrilow, G., *Chemische (stromlose) Vernickelung. Eugen G*. 1974, Leuze Verlag, Saulgau.

40. Pederson, L., *Comparison of stannous and stannic chloride as sensitizing agents in the electroless deposition of silver on glass using X-ray photoelectron spectroscopy.* Solar Energy Materials, 1982. **6**(2): p. 221-232.

41. Kim, J.J., S.-K. Kim, and Y.S. Kim, *A novel method for Cu electrodeposition on indium tin oxide aided by two-step Sn-Pd activation.* Japanese journal of applied physics, 2003. **42**(9A): p. L1080.

42. Osaka, T., H. Nagasaka, and F. Goto, *An electron diffraction study on mixed PdCl2/SnCl2 catalysts for electroless plating.* Journal of The Electrochemical Society, 1980. **127**(11): p. 2343-2346.

43. Schlesinger, M. and J. Kisel, *Effect of Sn (II)-Based Sensitizer Adsorption in Electroless Deposition.* Journal of The Electrochemical Society, 1989. **136**(6): p. 1658-1661.

44. Minjer, C.H.D. and P. Boom, *Nucleation with $SnCl_2$-$PdCl_2$ solutions of glass before electroless plating.* Journal of the Electrochemical Society, 1973. **120**(12): p. 1644-1650.

Figures

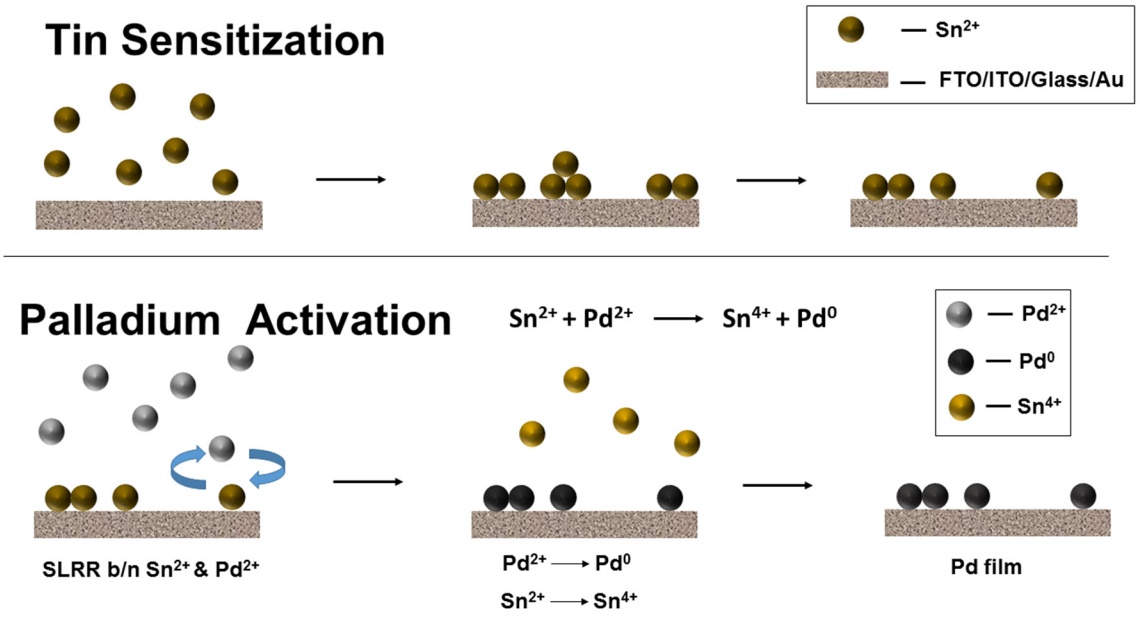

Figure 3.1: Schematic for Sn sensitization followed by palladium activation

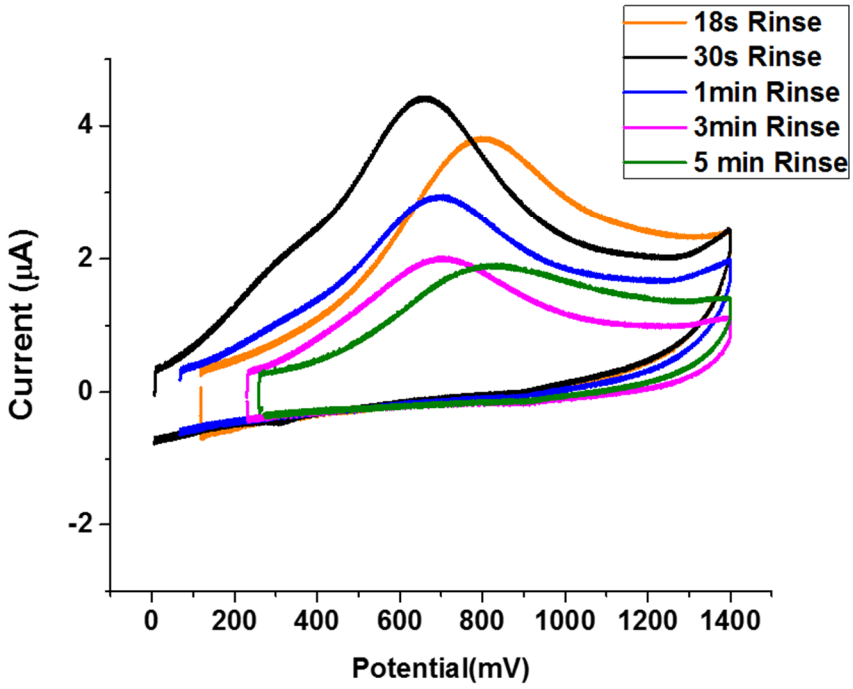

Figure 3.2: Oxidation of Sn^{2+} ions adsorbed on FTO from a 10 mM $SnCl_2$ and 0.1 M HCl solution by scanning from OCP to 1400 mV at 10 mV/s in 0.1 M H_2SO_4

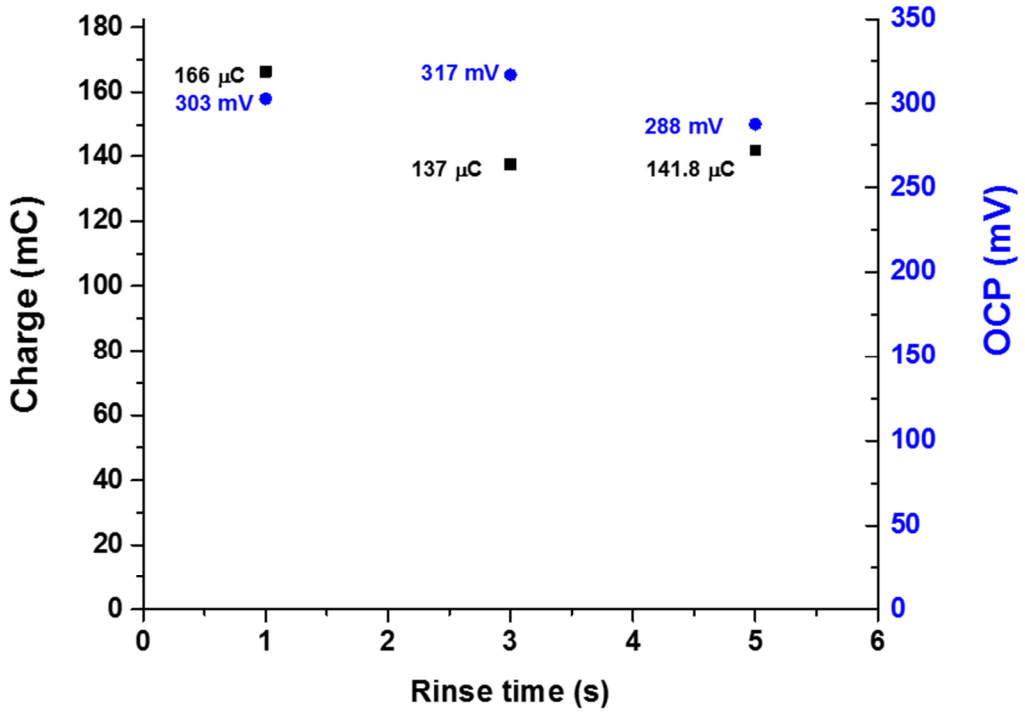

Figure 3.3: Effect of rinse time on oxidation of Sn^{2+} adsorbed from 10 mM $SnCl_2$ in 0.1 M HCl. Charges obtained by stepping from OCP to 1400 mV

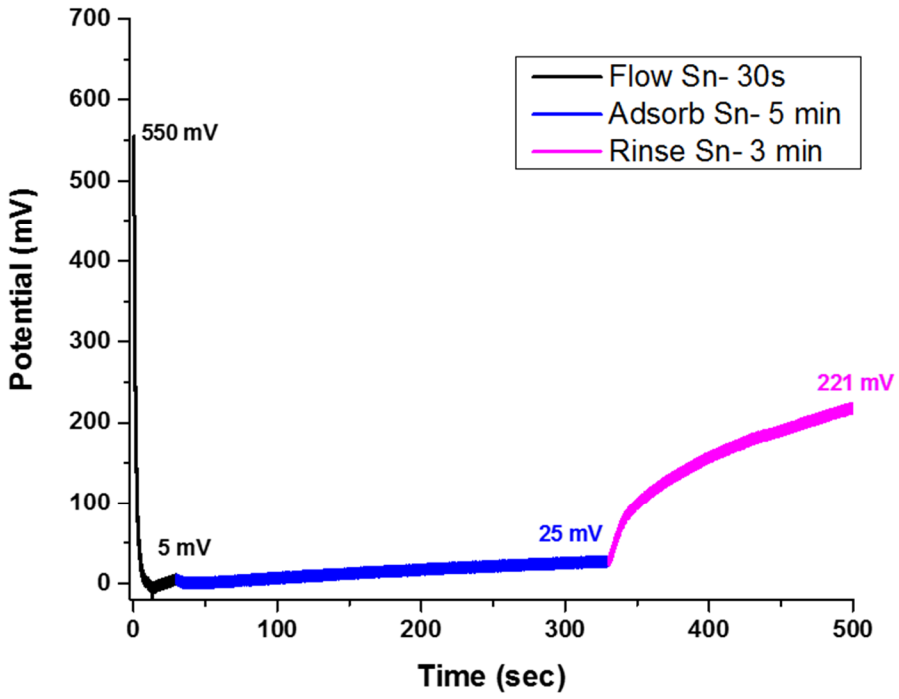

Figure 3.4: Potential-time trace for adsorption of Sn^{2+} ions on a clean FTO surface

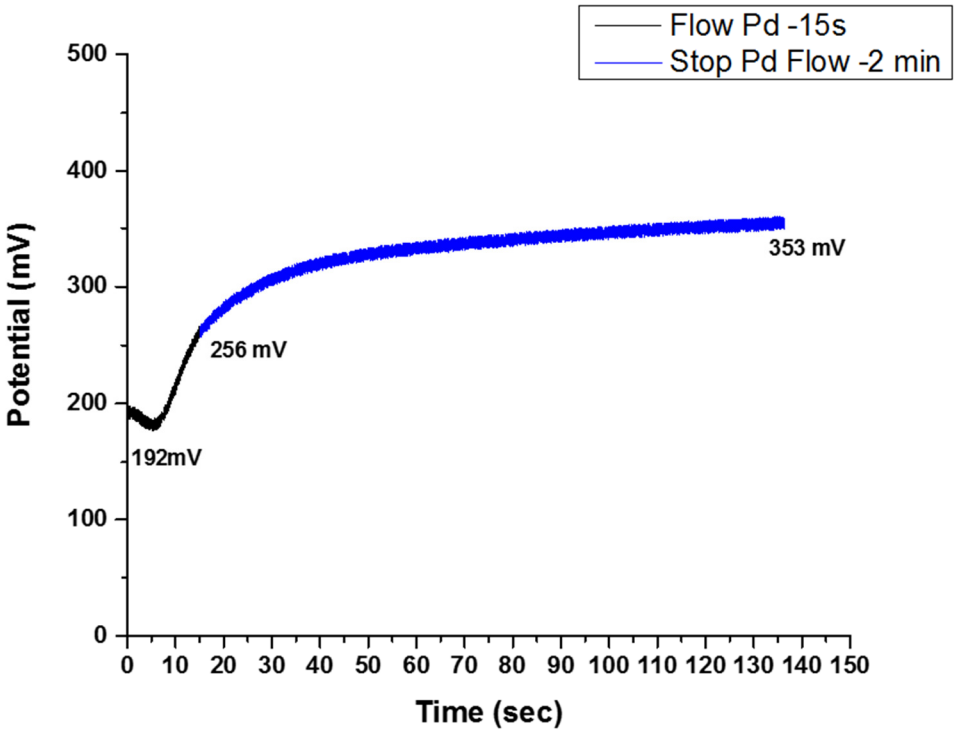

Figure 3.5: Potential-time trace for replacement of adsorbed Sn^{2+} ions by Pd

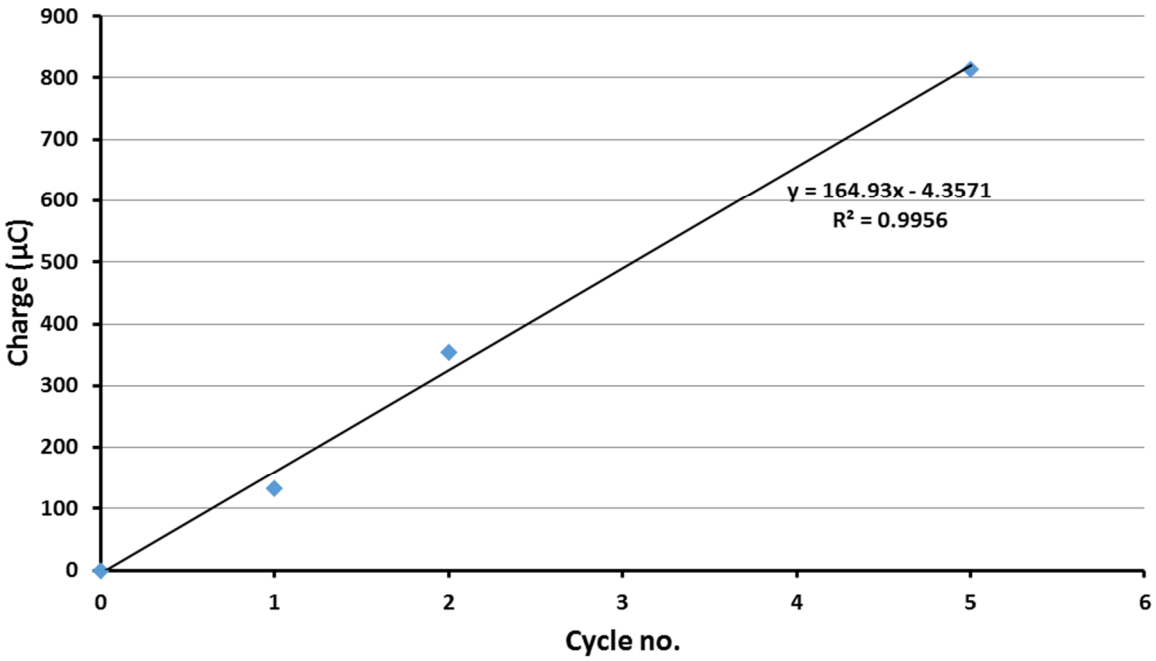

Figure 3.6: Linearity of EL-ALD on FTO indicating consistency in Pd deposition cycles

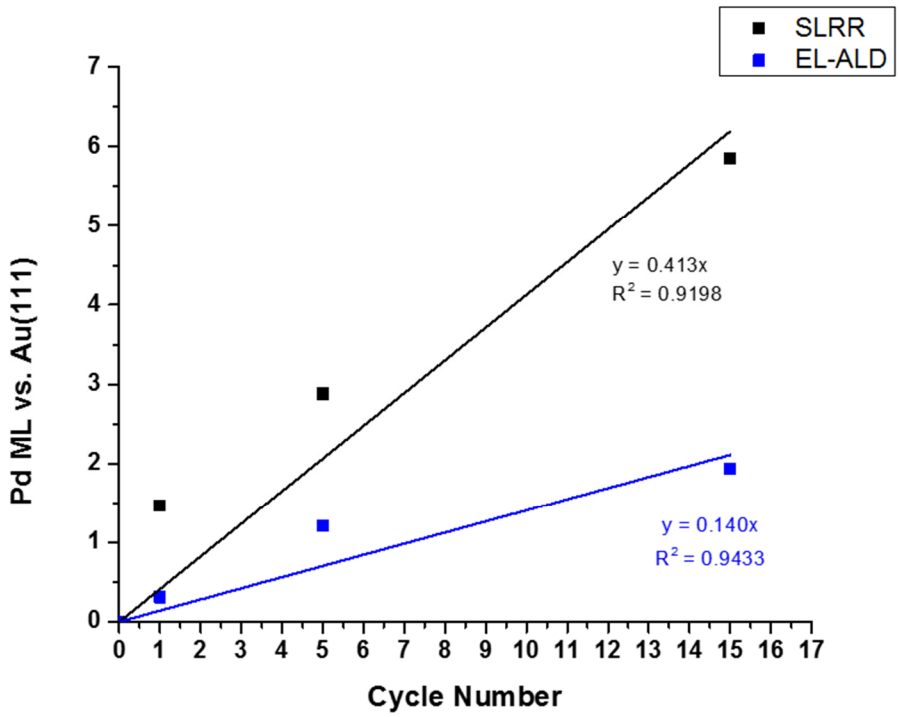

Figure 3.7: Comparison of E-ALD and EL-ALD on Au showing 3 times more deposition by E-ALD

a)

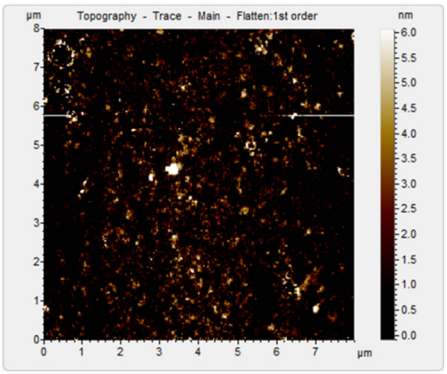

b)

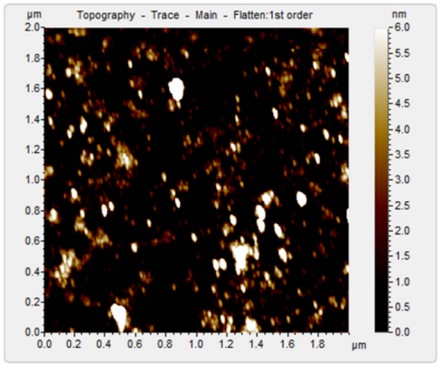

c)

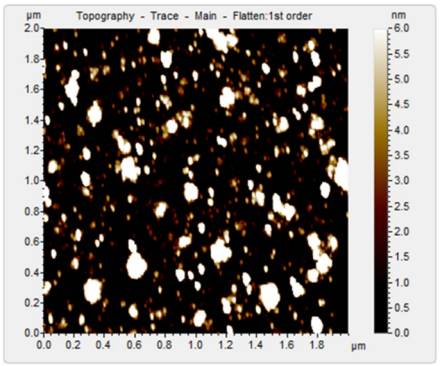

Figure 3.8: AFM images of Pd on glass. (a) Blank slide, (b) After 5 cycles of Pd deposition, (c) After 10 cycles of Pd deposition

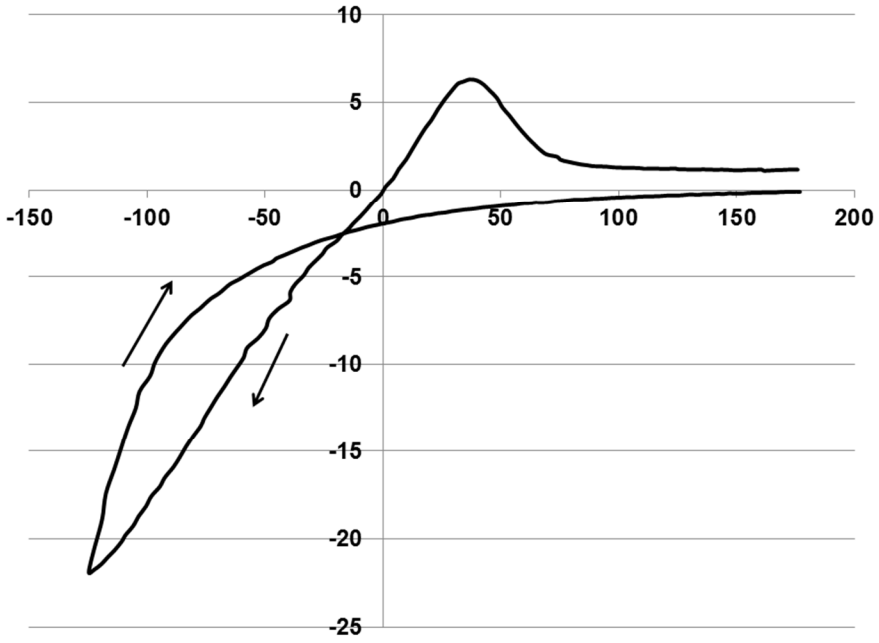

Figure 3.9: CV of an FTO slide in 1 mM $CuSO_4$ and 0.1 M H_2SO_4 at 10 mV/s

.

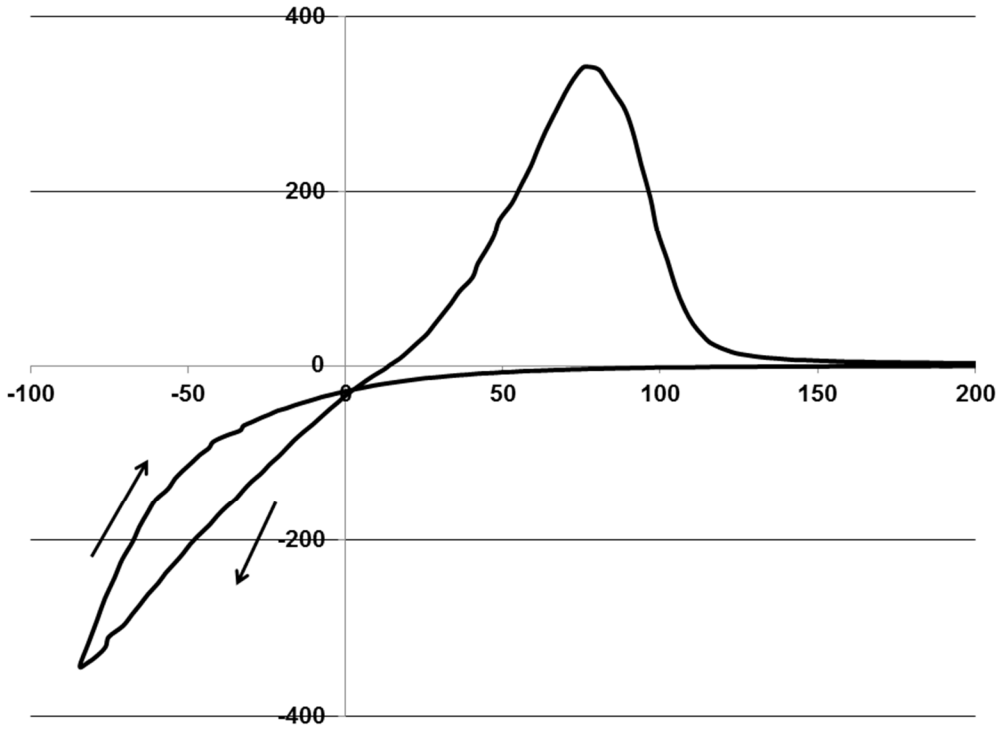

Figure 3.10: CV of an ITO slide in 1 mM $CuSO_4$ and 0.1 M H_2SO_4 at 10 mV/s

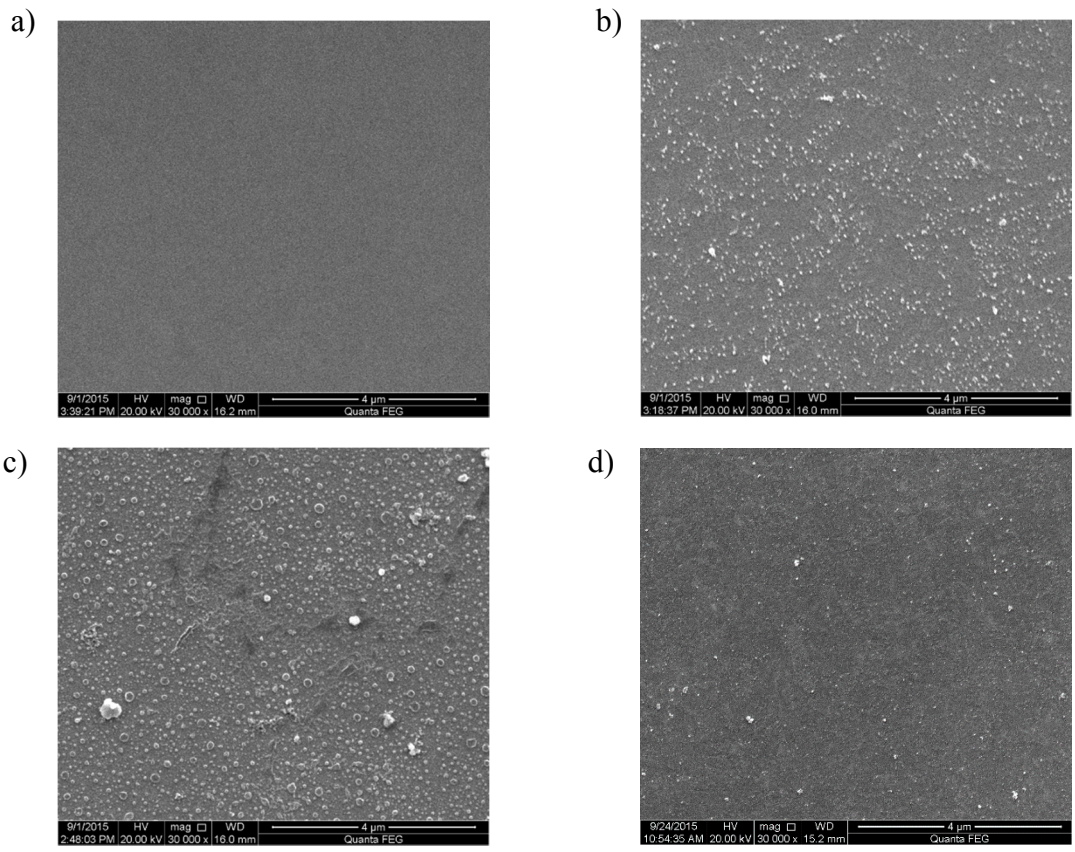

Figure 3.11: SEM images for Cu electrodeposition. (a) Bare ITO slide, (b) Cu directly deposited on ITO, (c) Cu deposited on a Pd sensitized, 10 mM Sn solution activated ITO slide, (d) Cu deposited on Pd sensitized, 1 mM Sn solution activated ITO

CHAPTER 4

CONCLUSIONS AND FUTURE OUTLOOK

This dissertation describe thin film deposition of Pd nanofilms and surface modification with Pt. The films have been used to investigate fundamental mechanisms like hydrogen sorption and oxygen reduction. In addition, an electroless method of deposition has been developed and preliminary results are discussed.

Chapter 2 describes Pd thin film deposition on polycrystalline Au (using Cu_{UPD} as a sacrificial metal) by a previously optimized E-ALD sequence. Surface modification of the films with Pt was also achieved similarly by SLRR of UPD Cu deposited on the Pd surfaced. The amount of Pt that was deposited was varied by tuning the Cu UPD potential. The bare Pd and Pt surface modified Pd thin films were then used to investigate hydrogen absorption, adsorption and desorption using cyclic voltammetry and coulometry. Based on the current time curves, significant enhancements in desorption currents, from the films were achieved which corresponded to faster reaction rates. Curve fitting was performed on the hydrogen oxidation current vs. time curves and the resultant time constants indicated the presence of two parallel processes corresponding to hydrogen adsorption and absorption. In conjunction with the destabilisation of surface hydride evident from the cyclic voltammograms, an indirect mechanism for hydrogen sorption is proposed. In this scenario, hydrogen molecules diffuse to the surface of the electrode. They then dissociate and are adsorbed by the Pd. In the next step, the adsorbed

atoms diffuse into the bulk of the films. The presence of Pt on the surface aids the absorption by destabilising the surface hydride leading to faster absorption into the films. This is in contrast to the direct mechanism discussed in the literature where absorption is proposed to occur in a single step.

Hydrogen storage was also considered and it was shown the despite Pt being present on the surface, the ability of the Pd films to store hydrogen was unaffected. This is especially significant when compared to alloys because they tend to lose the ability to store hydrogen with increasing Pt content. It will be interesting to see how the Pt-Pd films' ability to store hydrogen is affected when the Pt is present in between the Pd film instead of the surface. Another possible experiment would be to anneal the Pt-Pd surface. This should result in intercalation of the Pt ions into the Pd surface layer, forming a surface alloy. Experiments on hydrogen sorption in these constructs could help provide a more complete picture.

Appendix A describes using the Pt-Pd system described above for studying the ORR. The reaction is of fundamental importance in fuel cells. Preliminary studies indicate a reproducibility in the amount of oxygen reduced by the Pd films. Surface modification showed a reduction in the overpotential for reducing oxygen indicating a kinetic effect of the Pt that is present on the surface.

Chapter 3 describes an electroless method for the deposition of Pd on conducting, semi conducting and insulated surfaces. The deposition is a two-step sensitization and activation process. Initially, Sn ions are adsorbed on the substrate and then Pd ions are flowed in. Since Pd is a more noble metal than Sn, a galvanic exchange takes place resulting in Pd metal deposition. The length of rinse time between the sensitization and the activation step is very important. Too much rinsing will result in excess waste generation and also increase the time duration of the sequence significantly. Too little rinsing will result in weakly bound Sn ions present on the surface that could interfering with efficient Pd deposition on the surface. By comparing multiple rinse times, a three minute rinse was found to be optimal for our system. Initial results are promising indicated by the linearity in the amount of Pd deposited per cycle being similar to an E-ALD process. In order to get a more direct comparison between E-ALD and EL-ALD, Pd deposition was carried out on polycrystalline Au substrates. The results indicated a linearity in both the processes. However, the amount of Pd was almost three times more with electrodeposition than with electroless deposition. AFM imaging was carried out on glass and revealed the presence of islands that increase with an increase in deposition cycles. At present, the size distribution is slightly inhomogeneous on the glass surface. The AFM indicates that, at least on glass, the deposits grow via a nucleation and growth model. Thicker deposits on glass will need to be analysed to see if these islands eventually coalesce to form a film. One way of getting a more even

distribution would be to functionalise the glass slides and make the surface negatively charged, prior to adsorption of Sn ions. This should result in a better distribution of Sn ions and consequentially, Pd metal. There is of course a risk of the Sn ions strongly adsorbing onto the surface. This could make replacement by the Pd difficult. Comparable AFM images on TCOs will give a better picture of how the substrates influence the growth model. In addition, resistivity measurements can be used to track the change in conductance as the substrates become more metallic. Another method of evaluating the amount of Pd present on conductive substrates, if the deposits are thick enough, is by absorption of hydrogen. The amount of Pd can be indirectly calculated from the amount of hydrogen stored in the film assuming a theoretical H/Pd ratio of 0.7 (as was calculated in Chapter 2).

The Pd deposits can be used as a base for deposition of other metals. Cu electrodeposition was carried out on Pd activated ITO substrates. SEM imaging seems to suggest a detrimental effect for Cu deposition on these substrates. One possible reason could be the extremely high potentials that were chosen for depositing Cu. It is possible that the very high currents were too harsh for the underlying Pd activated ITO surface resulting in abnormal features and absence of deposition. Deposition at lower potentials could give an insight if this really is the case. To summarise, there are clearly more investigations that need to be carried out in order to develop a better understanding of the deposition process and the influence of the substrate. A method for depositing atomic layers and preventing formation of islands will need to be researched. However, the fact

the deposition is possible on such a wide variety of substrates indicates the versatility of the technique. The ability to control the amount of Pd deposited each cycle is definitely encouraging.

Appendix A

ENHANCEMENT OF OXYGEN REDUCTION KINETICS ON PLATINUM MODIFIED PALLADIUM E-ALD NANOFILMS

Introduction

Current polymer membrane electrolyte fuel cells use hydrogen fuel and oxygen from air to produce electricity. Part of the membrane electrode assembly is a cathode where oxygen gets reduced to form protons and water. The reaction is catalyzed typically by Pt nanoparticles supported on carbon particles with a high surface area. Considering that Pt is a very costly metal, by reducing the amount of Pt used, it is possible to achieve significant savings in cost. In addition, the oxygen reduction reaction is slow and this affects the performance of these fuel cells. There are several attempts to address this issue. Binary catalysts consisting of precious and non-precious metals in combination with Pt help in reducing the amount of Pt used. Pd metal has been studied in this regard in conjunction with Pt. One advantage of using Pd is that the lattice constant of Pd is very similar to the lattice constant of Pt [1]. Various groups have shown that epitaxial growth of a binary system is hence possible [2, 3]. In addition, the tensile strain for Pd deposition on Pt will be very small. Greeley et al. have theoretically evaluated and proposed enhancements for the ORR with Pt alloys than with pure Pt [4]. The Pt-Pd nanofilms described in chapter 2 are used here to study the ORR. Cyclic voltammetry was used to investigate enhancements in the kinetics of the reaction.

Experimental

Vapor deposited Au on glass slides (100 nm Au on a 5 nm Ti adhesion layer) were used as substrates for all deposits (EMF Corporation). Solutions were prepared with 18 MΩ-cm ultrapure water (Milli-Q Advantage A10). The Pd solution was 0.1 mM ultrapure-grade $PdCl_2$ (Aldrich Chemicals) in 50 mM HCl, in which the tetrachloropalladate ion $PdCl_4^{2-}$ is expected to form. The Pt solution was 0.01 mM ultrapure-grade H_2PtCl_6 in 50 mM $HClO_4$. The Cu solution was 1 mM $CuSO_4$ and 0.1 M H_2SO_4. Cyclic voltammetry for O_2 reduction was carried out in O_2 saturated 0.1 M H_2SO_4. The deposits were grown and studied in an automated electrochemical flow deposition system (Electrochemical ALD L.C., Athens, GA), diagramed in Figure A.1. The system consisted of five solution reservoirs, 5 valves and a variable speed peristaltic pump. The valves were housed in a Plexiglas box along with the solution reservoirs so they could be purged continuously with N_2, to minimize exposure to O_2. An additional sixth solution reservoir was connected to an O_2 tank (Airgas). The electrochemical flow cell, downstream from the valves, was also made of Plexiglas and had a volume of around 0.15 mL. A three electrode cell configuration was used, with a gold wire auxiliary electrode embedded in the front cell plate, directly across from the substrate. The reference was an Ag/AgCl electrode (3 M KCl) from Bioanalytical systems, against which potentials have been reported. E-ALD software "Sequencer-4" was used to control valves, pump and potentials. The Au on glass substrates had an exposed area of 2.01 cm^2.

Results and Discussion:

Formation of nanofilms by E-ALD: Prior to deposition, the Au substrate was cleaned by cycling in N_2 purged 0.1 M H_2SO_4 from -0.2 V to 1.4 V 3 times at 10 mV/s, followed by 2 cycles in 50 mM HCl from -0.2 V to 0.7 V at 10 mV/s, to produce a more ordered surface [5]. The E-ALD cycle for Pd deposition was optimized and studied previously by this group [5-8]. The sequence for Pd deposition and surface modification is the same as described in chapter 2. Briefly, Cu was deposited at an underpotential of 150 mV resulting in an atomic layer. This is followed by a redox replacement of the Cu by Pd^{2+} ions at open circuit resulting in an atomic layer of Pd metal. After multiple cycles of Pd deposition, Cu was again deposited on the surface of the Pd films and then replaced with Pt^{4+} ions with every two Cu atoms being replaced by a Pt atom. The amount of Pt deposited was controlled by varying the UPD potential.

Figure A.2 shows a CV of two different 5 cycle deposits of Pd. The cell was filled with O_2 saturated 0.1 M H_2SO_4 and then the pump was turned off. The potential was then scanned from OCP in the negative direction to 0 mV at 5 mV/s. There is a distinct reduction peak at -350 mV that is not present in CVs with N_2 purged 0.1 M H_2SO_4. Hence this peak can be ascribed to the reduction of oxygen. Figure A.3 compares CVs for bare Pd and Pd modified with 1, 3 and 6 cycles of Pt on the surface. There is a gradual decrease in the position of the reduction peaks with an increase in the amount of Pt. This is because Pt on the surface makes it easier for the O_2 reduction, indicating a surface process. Similar enhancements have been reported by others for monolayer (ML) catalysts. Adzic et al. have studied the ORR activity on Pd on Pt(111) surfaces and found the activity to be higher than Pd on Ru, Rh and Au(111) surfaces [9]. Bard et al., while

determining thermodynamic guidelines for designing binary catalysts and report an approach where one metal breaks the bond between the two oxygen atoms and the other reduces the adsorbed atomic oxygen [10]. Yang et al. describe a mechanism where the presence of adsorbed OH species on pure Pt hinders the ORR, while the presence of a binary electrode helps improve the kinetics due to a lower adsorbed -OH species coverage [11]. Vukmirovic et al. attribute the enhanced activity for ORR in hollow Pd-Pt structures to an increase in the number of high coordination sites [12]. Adzic et al. have described a four electron reduction for ORR on Pt/Pd and Pd/Pt/C nanoparticles, with trace amounts of H_2O_2 detected on their electrode surface [13].

ORR in aqueous solution can occur either through a 4 electron pathway or a 2 electron pathway [14]. The byproduct of the first pathway is H_2O and the latter is H_2O_2. Climent et al. indicate that the presence of adsorbed bisulfate anions could also influence the reaction [15]. Naohara et al. have reported similar reduction peaks at the same potentials for Pd on Au(111) surfaces and attribute it to a 2 electron pathway. Based on the literature and the shape and position of the reduction peaks in the voltammetry, we can assume that the reduction in 0.1 M H_2SO_4 could possibly follow a two electron reduction forming H_2O_2.

Conclusions

Pt modified Pd nanofilms were deposited on polycrystalline Au substrates by E-ALD. Cyclic voltammetry in O_2 saturated 0.1 M H_2SO_4 showed a distinct reduction peak for oxygen reduction. Based on the results present in the literature, this could be attributed to a 2 electron reduction of oxygen to H_2O_2. Surface modification with Pt led to a decrease in the overpotential for the reaction indicating a kinetic enhancement.

References

1. Peng, Z. and H. Yang, *Synthesis and Oxygen Reduction Electrocatalytic Property of Pt-on-Pd Bimetallic Heteronanostructures.* Journal of the American Chemical Society, 2009. **131**(22): p. 7542-7543.
2. Habas, S.E., et al., *Shaping binary metal nanocrystals through epitaxial seeded growth.* Nature materials, 2007. **6**(9): p. 692-697.
3. Lee, H., et al., *Localized Pd overgrowth on cubic Pt nanocrystals for enhanced electrocatalytic oxidation of formic acid.* Journal of the American Chemical Society, 2008. **130**(16): p. 5406-5407.
4. Greeley, J., et al., *Alloys of platinum and early transition metals as oxygen reduction electrocatalysts.* Nature chemistry, 2009. **1**(7): p. 552-556.
5. Sheridan, L.B., et al., *Hydrogen Adsorption, Absorption, and Desorption at Palladium Nanofilms formed on Au(111) by Electrochemical Atomic Layer Deposition (E-ALD): Studies using Voltammetry and In Situ Scanning Tunneling Microscopy.* Journal of Physical Chemistry C, 2013. **117**(30): p. 15728-15740.
6. Sheridan, L.B., et al., *Electrochemical Atomic Layer Deposition (E-ALD) of Palladium Nanofilms by Surface Limited Redox Replacement (SLRR), with EDTA Complexation.* Electrocatalysis, 2012. **3**(2): p. 96-107.
7. Sheridan, L.B., et al., *Formation of Palladium Nanofilms Using Electrochemical Atomic Layer Deposition (E-ALD) with Chloride Complexation.* Langmuir, 2013. **29**(5): p. 1592-1600.

8. Sheridan, L.B., et al., *Hydrogen sorption properties of bare and Rh-modified Pd nanofilms grown via surface limited redox replacement reactions.* Electrochimica Acta, 2014. **128**(0): p. 400-405.

9. Shao, M.H., et al., *Palladium Monolayer and Palladium Alloy Electrocatalysts for Oxygen Reduction†.* Langmuir, 2006. **22**(25): p. 10409-10415.

10. Fernández, J.L., D.A. Walsh, and A.J. Bard, *Thermodynamic guidelines for the design of bimetallic catalysts for oxygen electroreduction and rapid screening by scanning electrochemical microscopy. M-Co (M: Pd, Ag, Au).* Journal of the American Chemical Society, 2005. **127**(1): p. 357-365.

11. Peng, Z. and H. Yang, *Designer platinum nanoparticles: Control of shape, composition in alloy, nanostructure and electrocatalytic property.* Nano Today, 2009. **4**(2): p. 143-164.

12. Vukmirovic, M., et al. *Pt monolayer shell on hollow Pd core electrocatalysts: Scale up synthesis, structure, and activity for the oxygen reduction reaction*. in *Meeting Abstracts*. 2014. The Electrochemical Society.

13. Zhang, J., et al., *Platinum monolayer electrocatalysts for O2 reduction: Pt monolayer on Pd (111) and on carbon-supported Pd nanoparticles.* The Journal of Physical Chemistry B, 2004. **108**(30): p. 10955-10964.

14. Wroblowa, H.S. and G. Razumney, *Electroreduction of oxygen: a new mechanistic criterion.* Journal of Electroanalytical Chemistry and Interfacial Electrochemistry, 1976. **69**(2): p. 195-201.

15. Climent, V., N.M. Marković, and P.N. Ross, *Kinetics of Oxygen Reduction on an Epitaxial Film of Palladium on Pt(111).* The Journal of Physical Chemistry B, 2000. **104**(14): p. 3116-3120.

Figures

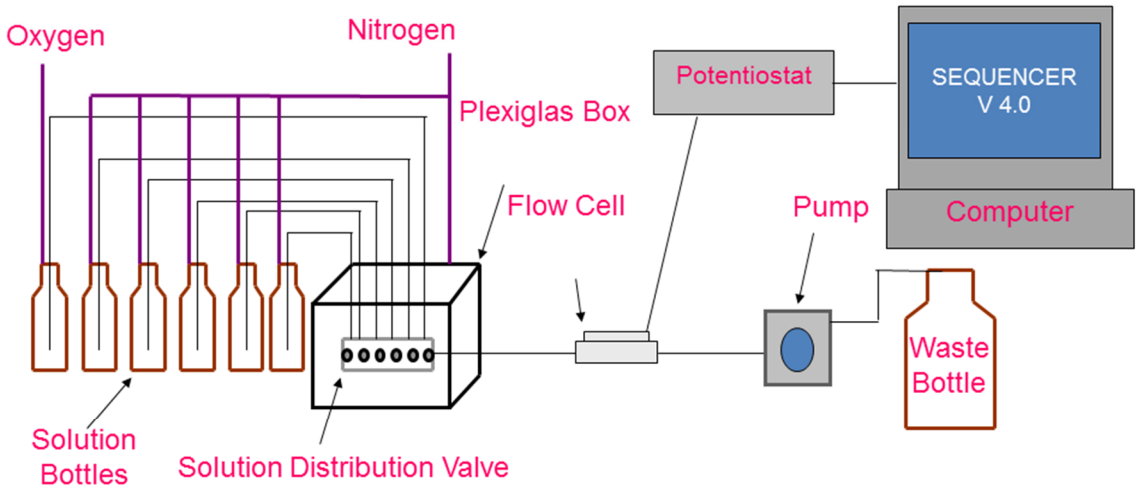

Figure A.1: Schematic of an E-ALD flow cell system modified for ORR

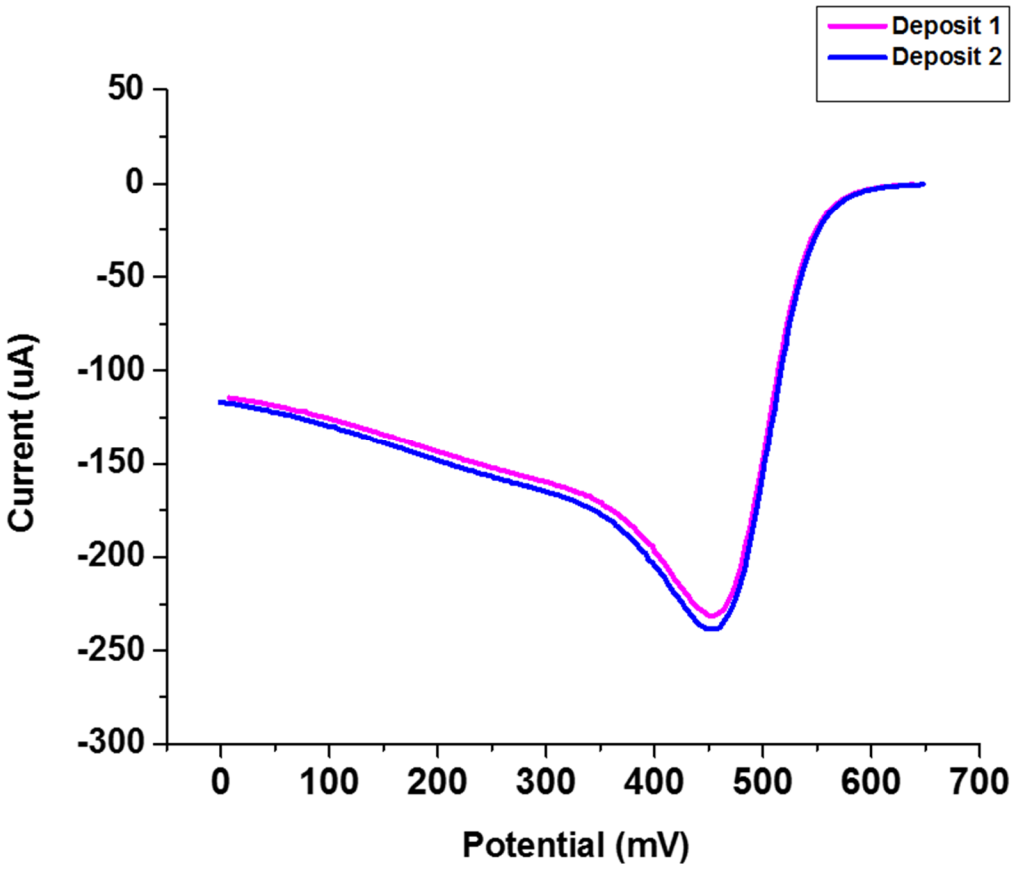

Figure A.2: CV of 5 cycles of Pd in O_2 saturated 0.1 M H_2SO_4 at 5 mV/s

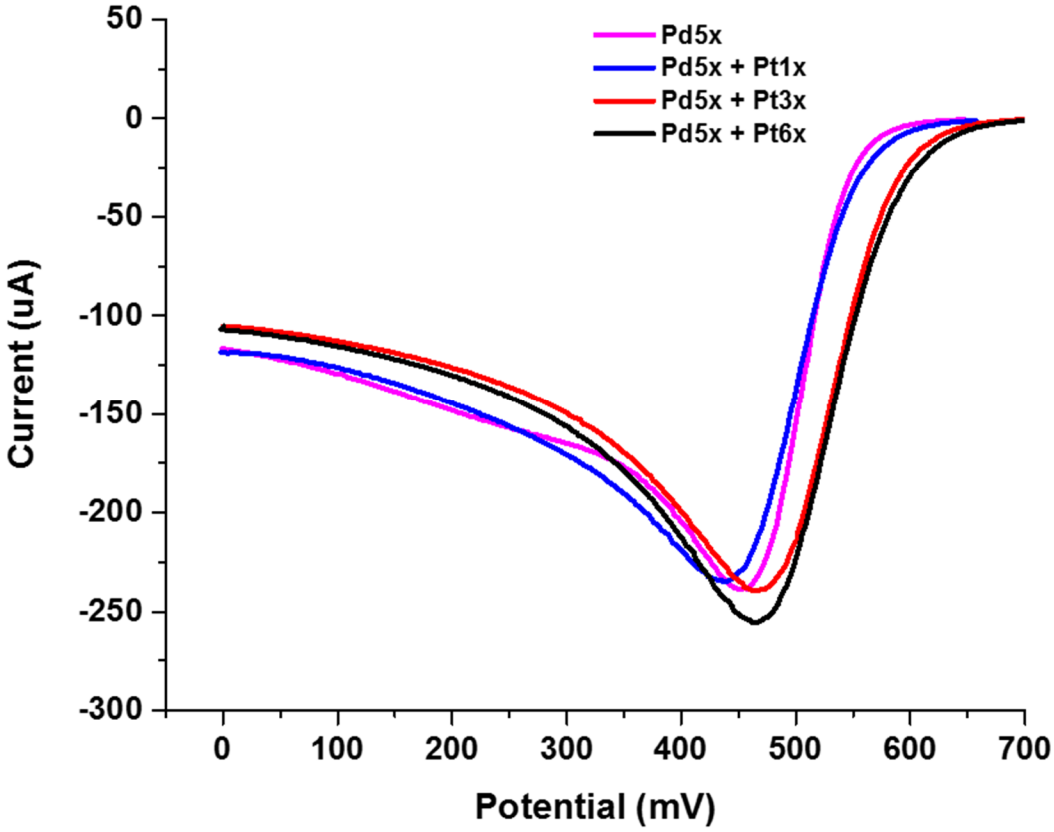

Figure A.3: CV of 5 cycles of Pd, modified with 1, 3 and 6 cycles of Pt in O_2 saturated 0.1 M H_2SO_4 at 5 mV/s